

# GEOMETRIC ANALYSIS OF POPULATION RHYTHMS IN SYNAPTICALLY COUPLED NEURONAL NETWORKS

J. Rubin and D. Terman

Dept. of Mathematics; Ohio State University; Columbus, Ohio 43210

## Abstract

We develop geometric dynamical systems methods to determine how various components contribute to a neuronal network's emergent population behavior. The results clarify the multiple roles inhibition can play in producing different rhythms. Which rhythms arise depends on how inhibition interacts with intrinsic properties of the neurons; the nature of these interactions depends on the underlying architecture of the network. Our analysis demonstrates that fast inhibitory coupling may lead to synchronized rhythms if either the cells within the network or the architecture of the network is sufficiently complicated. This cannot occur in mutually coupled networks with simple cells; the geometric approach helps explain how additional network complexity allows for synchronized rhythms in the presence of fast inhibitory coupling. The networks and issues considered are motivated by recent models for thalamic oscillations. The analysis helps clarify the roles of various biophysical features, such as fast and slow inhibition, cortical inputs and ionic conductances, in producing network behavior associated with the spindle sleep rhythm and with paroxysmal discharge rhythms. Transitions between these rhythms are also discussed.

Key words: oscillations, inhibition, synchronization, synaptic coupling, singular perturbation

## 1. Introduction.

Neuronal networks often exhibit a rich variety of oscillatory behavior. The dynamics of even a single cell may be quite complicated; it may, for example, fire repetitive spikes or bursts of action potentials that are each followed by a silent phase of near quiescent behavior [22,41]. The bursting behavior may wax and wane on a slower time scale [1,5]. Examples of population rhythms include synchronous behavior, in which every cell in the network fires at the same time, and clustering, in which the entire population of cells breaks up into subpopulations or blocks; the cells within a single block fire synchronously while different blocks are desynchronized from each other [13,19]. Of course, much more complicated population rhythms are also possible [34,36]. Activity may also propagate through the network in a wave-like manner [7,14,18,23].

A network's population rhythm results from interactions between three separate components: the intrinsic properties of individual neurons, the synaptic properties of coupling between neurons, and the architecture of coupling (i.e., which neurons communicate with each other). These components typically involve numerous parameters and multiple time scales. The synaptic coupling, for example, can be excitatory or inhibitory, and its possible turn on and turn off rates can vary widely. Neuronal systems may include several different types of cells as well as different types of coupling. An important and typically very challenging problem is to determine the role each component plays in shaping the emergent network behavior.

In this paper we consider recent models for thalamic oscillations [6,8,14,15,28,29,30,33,44]. The networks consist of several types of cells and include excitatory as well as both fast and slow inhibitory coupling. One interesting property of these networks is that they exhibit very different rhythms for different parameter ranges. For some parameter values, the network behavior resembles that of the spindle sleep rhythm: one population of cells is synchronized at the spindle frequency while another population of cells exhibits clustering. If a certain parameter, corresponding to the strength of fast inhibition, is varied, then the entire network becomes synchronized. This resembles paroxysmal discharge rhythms associated with spike-and-wave epilepsy. In other parameter ranges, the network behavior is similar to that associated with the delta sleep rhythm; in this case, each cell exhibits an entirely different behavior from before.

We develop geometric dynamical systems methods to analyze the mechanisms responsible for each of these rhythms and for the transitions between them. This approach helps determine each component's contribution to the network behavior and to clarify how the behavior changes with respect to parameters. We are particularly interested in analyzing the role of inhibitory coupling in generating different oscillatory behaviors. This is done by considering a series of networks with increasing levels of complexity. Our analysis demonstrates, for example, how networks with distinct architectures can make different uses of inhibition to produce different rhythms. The techniques we develop are quite general and do not depend on the details of the specific systems. For a given network, however, these techniques lead to rather precise conditions for when a particular rhythm is possible.

Many papers have considered the role of inhibition in synchronizing oscillations [2,9,10,11,12,21,24,25,32,37,38,42,43,45,46]. One conclusion of some of these papers is that inhi-

bition can lead to synchrony only if the inhibition decays at a sufficiently slow rate [32,43]; in particular, the rate of decay of the synapses must be slower than the rate at which the neurons recover in their refractory period. These theoretical studies, however, have considered very idealized networks that include rather simple models for both the individual neurons and the architecture of synaptic coupling. By considering more realistic biophysical models, we demonstrate that fast inhibitory coupling can indeed lead to synchronous rhythms. We show that this is possible both in networks which include complicated cells, but simple architectures, and in networks with more complicated architectures, but simple cells.

Geometric singular perturbation methods have been used previously to study the population rhythms of neuronal networks [20,26,27,32,34,35]. The relevant networks each possess different time scales; this allows one to dissect the full system into fast and slow subsystems. The advantage of this approach is that the fast and slow subsystems are of lower order than the original system. If the cells are homogeneous, then one can make a further reduction by viewing all the oscillators as points evolving in a single phase space. The dimension of this phase space equals the total number of slow intrinsic and slow synaptic variables corresponding to a single cell.

There are two crucial issues related to this analysis. The first is concerned with the existence of a singular solution corresponding to a particular pattern. We assume that individual cells, without any coupling, are unable to oscillate. The existence of network oscillatory behavior then depends on whether the singular trajectory is able to ‘escape’ from the silent phase. An important point will be that greater cellular or network complexity enhances each cell’s opportunity to escape the silent phase when coupled. The second issue is concerned with the stability of the solution. We must demonstrate that the trajectories corresponding to different cells are brought closer together as they evolve in phase space. As we shall see, this compression is usually not controlled by one single factor; it depends on the underlying architecture as well as nontrivial interactions between the intrinsic and synaptic properties of the cells (see also [32]). Our analysis demonstrates, for example, why thalamic networks are well suited to use inhibitory coupling both to help synchronize oscillations and to produce other, clustered, rhythms.

An outline of the paper is the following. In the next section we describe, in detail, the types of networks to be considered. We will distinguish between simple and complex cells. As a concrete example, we consider recent conductance based models for thalamocortical relay (TC) cells [8,14]. Complex cells can be realized as a model for a TC cell which includes three ionic currents: a low threshold calcium current ( $I_T$ ), the non-selective sag current ( $I_h$ ) and a leak. A simple cell does not include  $I_h$ . In this context, our results help to explain the role of  $I_h$  in generating network activity; we shall see that this role depends on the architecture of the network. We also discuss different forms of synaptic coupling and different architectures to be considered later.

In Sections 3 and 4 we consider a series of networks in order to understand when mutually coupled inhibitory networks can produce synchronized rhythms. Synchrony is not possible in networks with simple cells and fast synapses and in Section 3 we explain why. This analysis helps to motivate what ingredients are needed for synchronization. In

Section 4 we show that synchronization is possible in mutually coupled networks which include complex cells and fast synapses. This analysis is similar to that in [32], where it was shown that synchronization is possible in networks with simple cells and slow inhibitory coupling. Those networks contain two types of slow processes: one corresponds to an intrinsic ionic current and the other to a synaptic slow variable. The main conclusion of the analysis here is that what is crucial for synchronization is that the network possess at least two slow processes; one may be intrinsic and the other synaptic or both may be intrinsic.

In Sections 5 and 6, we consider networks with architectures motivated by recent models for the spindle sleep rhythm. The more complex architectures allow the network to use inhibition in different ways to produce different population rhythms. In particular, inhibition can play an important role in synchronizing the rhythms in a much more robust way than in the mutually coupled networks. We will demonstrate how tuning various parameters allows the network to control the effect of inhibition and thereby control the emergent behavior.

Consequences of these results for the full thalamic networks are presented in Section 7. We consider the roles of various biophysical parameters associated with fast and slow inhibition, the sag current, cortical inputs, and other currents. These results help clarify both the mechanisms responsible for the spindle, delta, and paroxysmal discharge rhythms and the ways that changes in biophysical parameters lead to transitions between different rhythms. We conclude with a discussion in Section 8.

## 2. The Models.

We now present the models to be considered later. We begin by describing the equations corresponding to individual cells. We distinguish between what we call *simple cells* and *complex cells*. We then describe the synaptic coupling between two cells. It is necessary to explain which parameters determine whether the synapse is *excitatory* or *inhibitory* and which other parameters determine whether the synapse is *fast* or *slow*. It will also be necessary to distinguish between *direct synapses* and *indirect synapses*. Finally, we describe the types of architectures to be considered.

### A. Single Cells.

We model a *simple cell* as the relaxation oscillator

$$(2A.1) \quad \begin{aligned} v' &= f(v, w) \\ w' &= \epsilon g(v, w) \end{aligned}$$

Here  $\epsilon$  is assumed to be small. We assume that the  $v$ -nullcline,  $f(v, w) = 0$ , defines a cubic-shaped curve as shown in Fig. 1A, and the  $w$ -nullcline,  $g = 0$ , is a monotone decreasing curve which intersects  $f = 0$  at a unique point  $p_0$ . We also assume that  $f > 0$  ( $f < 0$ ) above (below) the  $v$ -nullcline and  $g > 0$  ( $< 0$ ) below (above) the  $w$ -nullcline. If  $p_0$  lies on the middle branch of  $f = 0$ , then (2A.1) gives rise to a periodic solution for all  $\epsilon$  sufficiently small and we say that the system is *oscillatory*. In the limit  $\epsilon \rightarrow 0$ , one can construct a singular solution as shown in Fig. 1A. If  $p_0$  lies on the left branch of  $f = 0$ , then the

system is said to be *excitable*;  $p_0$  is a stable fixed point and there are no periodic solutions for all  $\epsilon$  small. For some of our results, it will be necessary to make some further, more technical, assumptions on the nonlinearities  $f$  and  $g$ . We will sometimes assume that

$$(2A.2) \quad f_w > 0, \quad g_v < 0 \quad \text{and} \quad g_w < 0$$

near the singular solutions.

By a *complex cell* we mean one which contains at least two slow processes. We consider complex cells which satisfy equations of the form

$$(2A.3) \quad \begin{aligned} v' &= f(v, w, y) \\ w' &= \epsilon g(v, w) \\ y' &= \epsilon h(v, y) \end{aligned}$$

Precise assumptions required on the nonlinear functions in (2A.3) are given later. For now, we assume that for each fixed value of  $y$ , the functions  $f(v, w, y)$  and  $g(v, w)$  satisfy the conditions described above for a simple cell. Then  $\{f(v, w, y) = 0\}$  defines a cubic shaped surface. The system (2A.3) is said to be *excitable* if there exists a unique fixed point, which we denote by  $p_0$ , and this lies on the left branch of the cubic shaped surface. One can construct singular solutions of (2A.3) and one of these is shown in Fig. 1B. The singular solution shown begins in the silent phase, or left branch, of the surface. It evolves there until it reaches the curve of jump-up points which correspond to the left ‘knees’ of the cubic surface. The singular solution then jumps up to the active phase, or right branch, of the surface. It evolves in the active phase until it reaches the jump-down points or right ‘knees’ of the surface. It then evolves in the silent phase, approaching the stable fixed point at  $p_0$ . A more formal description of certain singular solutions is given in Section 4B.

## B. Synaptic Coupling.

Consider the network of two mutually coupled cells:  $E_1 \leftrightarrow E_2$ . The equations corresponding to this network are

$$(2B.1) \quad \begin{aligned} v_1' &= f(v_1, q_1) - g_{syn} s_2 (v_1 - v_{syn}) \\ q_1' &= \epsilon \Lambda(v_1, q_1) \\ v_2' &= f(v_2, q_2) - g_{syn} s_1 (v_2 - v_{syn}) \\ q_2' &= \epsilon \Lambda(v_2, q_2) \end{aligned}$$

Here,  $q_i = w_i$  and  $\Lambda = g$  if the cells are simple, while  $q_i = (w_i, y_i)$  and  $\Lambda = (g, h)$  if the cells are complex. In (2B.1),  $g_{syn} > 0$ . It is the parameter  $v_{syn}$  that determines whether the synapse is excitatory or inhibitory. If  $v_{syn} < v$  along each bounded singular solution, then the synapse is inhibitory.

The coupling arises in the synaptic variables  $s_i$ ,  $i = 1, 2$ . We consider two choices for the  $s_i$ . Each  $s_i$  may satisfy a first order equation of the form

$$(2B.2) \quad s_i' = \alpha(1 - s_i)H(v_i - \theta_{syn}) - \beta s_i$$

Here,  $\alpha$  and  $\beta$  are positive constants,  $H$  is the Heaviside step function and  $\theta_{syn}$  is a threshold above which one cell can influence the other. Note that  $\alpha$  and  $\beta$  are related to the rates at which the synapses turn on or turn off. For *fast synapses*, we assume that both of these constants are  $O(1)$  with respect to  $\epsilon$ . For a *slow synapse*, we assume that  $\alpha = O(1)$  and  $\beta = O(\epsilon)$ ; hence, a slow synapse activates on the fast time scale, but turns off on the slow time scale.

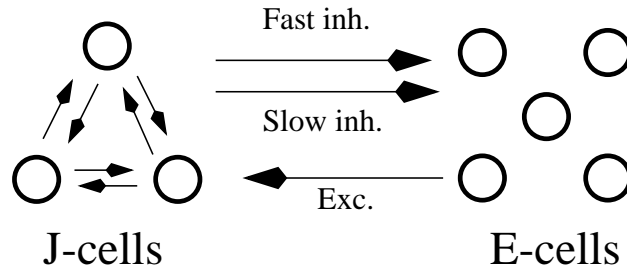
If the synaptic variables satisfy (2B.2), then we say that the synapse is *direct*. We will also consider *indirect synapses*. These are modeled by introducing a second synaptic variable  $x_i$ , as in [15,32]. The equations for  $(x_i, s_i)$  are:

$$(2B.3) \quad \begin{aligned} x_i' &= \epsilon \alpha_x (1 - x_i) H(v_i - \theta_{syn}) - \epsilon \beta_x x_i \\ s_i' &= \alpha (1 - s_i) H(x_i - \theta_x) - \beta s_i \end{aligned}$$

Here,  $\alpha_x$  and  $\beta_x$  are positive constants. Note that indirect synapses have the effect of introducing a delay in the synaptic action and this delay takes place on the slow time scale. If, say, the cell  $E_1$  fires, then  $x_1$  will activate once  $v_1$  crosses the threshold  $\theta_{syn}$ . The activation of  $s_1$  must wait until  $x_1$  crosses the second threshold  $\theta_x$ .

### C. Globally Inhibitory Networks.

Besides mutually coupled networks, we also consider networks with the following architecture:



This network contains two different types of cells; these are labeled as  $E$ -cells and  $J$ -cells. Each  $E$ -cell sends fast excitation to some of the  $J$ -cells and each  $J$ -cell sends inhibition to some of the  $E$ -cells. The inhibition may be fast or slow (or both). There is no communication among different  $E$ -cells; however, the  $J$ -cells communicate with each other via fast inhibitory coupling.

This network is motivated by recent models for sleep rhythms [8,44]. The  $E$ - and  $J$ -cells correspond to thalamocortical relay (TC) and thalamic reticularis (RE) cells, respectively. In Section 5, we consider networks with this architecture in which each  $E$ - and  $J$ -cell is modeled as a simple cell. In Sections 6 and 7, we consider more biophysical models for these cells.

### D. Singular Solutions.

All of the networks in this paper are analyzed by treating  $\epsilon$  as a small, singular perturbation parameter. The first step in this analysis is to identify the fast and slow variables.

We then dissect the full system of equations into fast and slow subsystems. The fast subsystem is obtained by simply setting  $\epsilon = 0$  in the original equations. This leads to a reduced set of equations for the fast variables with each of the slow variables constant. The slow subsystem is obtained by first introducing the slow time scale  $\tau = \epsilon t$  and then setting  $\epsilon = 0$  in the resulting equations. This leads to a reduced system of equations for just the slow variables, after solving for each fast variable in terms of the slow ones.

### 3. Mutually Coupled Simple Cells With Fast Inhibitory Synapses.

#### A. Introductory Remarks.

We now consider networks of two mutually coupled simple cells with fast inhibitory synapses. These networks cannot support stable synchronized oscillations (for small  $\epsilon$ ) and here we explain why. There are different reasons depending on whether the cells are excitable or oscillatory and whether the synapses are direct or indirect. We treat various cases separately. This analysis will help motivate the dynamical properties needed for a more complex network to achieve synchrony.

Here we derive the slow equations. For this, it will be convenient to introduce the following notation. Let  $F(v, w, s) \equiv f(v, w) - g_{syn}s(v - v_{syn})$ . We assume that for each  $s$ ,  $\{(v, w) : F(v, w, s) = 0\}$  defines a cubic-shaped curve denoted by  $\mathcal{C}_s$ . Denote the left and right branches of this cubic by  $\mathcal{L}_s \equiv \{v = \Phi_L(w, s)\}$  and  $\mathcal{R}_s \equiv \{v = \Phi_R(w, s)\}$ , respectively. It is natural to assume that  $\frac{\partial \Phi_R}{\partial w}$  and  $\frac{\partial \Phi_L}{\partial w}$  are both positive. Finally, let  $G_L(w, s) \equiv g(\Phi_L(w, s), w)$  and  $G_R(w, s) \equiv g(\Phi_R(w, s), w)$ .

For the case of simple cells with fast, direct synapses, the slow variables are  $w_1$  and  $w_2$ , while the fast variables are  $v_1, v_2, s_1$  and  $s_2$ . The slow equations are obtained by letting  $\tau = \epsilon t$  in (2B.1), (2B.2) and then setting  $\epsilon = 0$  in the resulting equation. This leads to the slow system

$$(3A.1) \quad \begin{aligned} 0 &= F(v_i, w_i, s_j) \\ \dot{w}_i &= g(v_i, w_i) \\ 0 &= \alpha(1 - s_i)H(v_i - \theta_{syn}) - \beta s_i \end{aligned}$$

Here,  $i = 1, 2$ ,  $j \neq i$ , and differentiation is with respect to  $\tau$ .

If cell  $i$  is silent, so that  $v_i < \theta_{syn}$ , then  $s_i = 0$  and  $(v_i, w_i)$  lies on the left branch of the cubic determined by  $s_j$ . That is,  $v_i = \Phi_L(w_i, s_j)$ . The slow evolution of  $w_i$  is given by the scalar equation

$$(3A.2) \quad \dot{w}_i = G_L(w_i, s_j)$$

If cell  $i$  is active, so that  $v_i > \theta_{syn}$ , then  $(v_i, w_i)$  lies on the right branch of the cubic determined by  $s_j$ . Hence,  $v_i = \Phi_R(w_i, s_j)$  and the slow evolution of  $w_i$  is given by

$$(3A.3) \quad \dot{w}_i = G_R(w_i, s_j)$$

From the last equation in (3A.1), it follows that  $s_i = \frac{\alpha}{\alpha + \beta} \equiv \sigma_A$  when cell  $i$  is active.

## B. Excitable Cells.

We assume throughout this subsection that the synapses are fast and both cells, without any coupling, are excitable. We will show that a singular periodic synchronous solution cannot exist if the synapses are direct. Such a solution may exist if the synapses are indirect, however it must be unstable.

If the synapses are direct, then, for a synchronous solution, each cell lies on  $\mathcal{L}_0$  during the silent phase. If the cells are excitable, then there exists a stable rest point on  $\mathcal{L}_0$  and each cell is attracted to this stable rest point. Hence, the cells can never jump up to the active phase and the synchronous periodic solution cannot exist.

If the synapses are indirect, then the cells lie on  $\mathcal{L}_{\sigma_A}$  immediately after jumping down from the active phase. They remain on this branch until the variables  $x_i$  fall below their threshold  $\theta_x$ . If this delay is long enough, then the cells may lie above the left knee of  $\mathcal{L}_0$  when they are released from inhibition. In this case, the cells jump up to the active phase and a synchronous periodic solution may exist. After the cells jump-up, each  $x_i$  rises above  $\theta_x$  with  $s_i$  still at  $\sigma_A$ ; this persists for the remainder of the oscillation. Such a singular solution appears in Fig. 2A.

Such a solution is unstable. If perturbed, then one of the cells, say cell 1, jumps up first when  $x_2$  falls to  $\theta_x$ . At this time, cell 2 lies in the silent phase with  $x_1 > \theta_x$ . After cell 1 jumps up,  $v_1 > v_{syn}$  and therefore  $x_1' > 0$ . Hence,  $s_1$  is fixed at  $\sigma_A$  and cell 2 cannot be released from the silent phase. Cell 2 must wait near the fixed point on  $\mathcal{L}_{\sigma_A}$  until cell 1 returns to the silent phase before it can jump up. This will eventually result in some form of asynchronous oscillation.

## C. Oscillatory Cells With Direct Synapses.

Now suppose that each cell is oscillatory; we still assume that the synapses are fast and direct. Then a synchronous periodic solution exists. The orbit lies on  $\mathcal{L}_0$  during the silent phase and lies on  $\mathcal{R}_{\sigma_A}$  during the active phase.

This solution is unstable for the following reason. Suppose both cells are initially very close to each other on  $\mathcal{L}_0$ . The cells then evolve on  $\mathcal{L}_0$  until one of the cells, say cell 1, reaches the left knee of  $\mathcal{L}_0$ . Cell 1 then jumps up to the active phase. When  $v_1$  crosses the threshold  $\theta_{syn}$ ,  $s_1$  switches from 0 to  $\sigma_A$  and cell 2 jumps from  $\mathcal{L}_0$  to  $\mathcal{L}_{\sigma_A}$ , as shown in Fig. 2B. This demonstrates that the cells are uniformly separated for arbitrarily close initial data. The synchronous solution must, therefore, be unstable.

## D. Oscillatory Cells With Indirect Synapses.

The synchronous solution is unstable for direct synapses because when one cell fires it immediately ‘steps on’ the other cell. If the synapses are indirect, then there is a delay from when one cell fires until the other cell feels the inhibition. This gives the second cell a ‘window of opportunity’ in which to fire. We claim, however, that the synchronous solution must still be unstable.

To simplify the analysis, we assume that the delay is a fixed constant  $\delta$ . By this we

mean the following. Consider the slow time scale  $\tau = \epsilon t$  and suppose that one cell, say cell 1, jumps up when  $\tau = \tau_0$ . Since  $v_1$  crosses  $\theta_{syn}$  on the fast time scale, this immediately activates the variable  $x_1$ . The delay corresponds to how long it takes  $x_1$  to cross  $\theta_x$ . We assume that  $x_1(\tau_0 + \delta) = \theta_x$ . The delay should actually depend on  $x_1(0)$ . The following analysis can be easily extended to that case.

To prove that the synchronous solution is unstable, we begin with both cells in the silent phase with one cell, say cell 1, at the left knee of  $\mathcal{L}_0$  ready to fire. We follow the singular solution around in phase space until the cells complete one cycle – that is, until one of the cells returns to the left knee of  $\mathcal{L}_0$ . We show that the ‘distance’ between the cells increases after this one cycle. By ‘distance’ we mean the following: If the cells lie on the same branch of the same cubic, then the distance between the cells is the time it takes for the trailing cell to evolve on that branch to the position of the leading cell. Note that as long as the cells remain on the same branch, this distance is invariant. Hence, any expansion in the distance must take place as the cells jump from one branch to another. Below, we focus on the sequence of events from the moment cell 1 jumps up until cell 2 jumps up and begins to inhibit cell 1. We demonstrate that there is expansion in the distance between the cells during this jumping up process; see also Fig. 2C. A similar argument holds for the jumping down process. Throughout this argument we consider the slow time scale  $\tau = \epsilon t$ . We denote the distance between the cells at time  $\tau$  as  $\rho(\tau)$ .

Suppose cell 1 jumps up when  $\tau = 0$ . Moreover, cell 2 begins so close to cell 1 that it reaches the left knee of  $\mathcal{L}_0$  and then fires at some time  $\tau_0 < \delta$ . After it jumps up, cell 2 lies on  $\mathcal{R}_0$  for  $\tau_0 < \tau < \delta$ . When  $\tau = \delta$ , cell 2 jumps from  $\mathcal{R}_0$  to  $\mathcal{R}_{\sigma_A}$ . Cell 1, on the other hand, lies on  $\mathcal{R}_0$  for  $0 < \tau < \tau_0 + \delta$ . It jumps from  $\mathcal{R}_0$  to  $\mathcal{R}_{\sigma_A}$  when  $\tau = \tau_0 + \delta$ . Hence, both cells lie on  $\mathcal{R}_{\sigma_A}$  when  $\tau = \tau_0 + \delta$  (see Fig. 2C). We claim that  $\rho(\tau_0 + \delta) > \rho(0)$ . This gives the desired expansion.

Note that  $\rho(0) = \tau_0$ . Both cells jump up at the left knee of  $\mathcal{L}_0$  to the same point on  $\mathcal{R}_0$  and then lie on  $\mathcal{R}_0$  for  $\tau_0 < \tau < \delta$ . Hence,  $\rho(\delta) = \rho(0)$ . The cells, however, lie on different branches for  $\delta < \tau < \tau_0 + \delta$ . The distance between the cells may then change because the rate at which a cell evolves depends on which branch the cell lies on. Note that cell 1 is the leading cell and it lies on  $\mathcal{R}_0$ . Hence, the distance between the cells will increase if the rate at which a cell evolves on  $\mathcal{R}_0$  is greater than the rate on  $\mathcal{R}_{\sigma_A}$ . We show that this is indeed the case.

According to (3A.3), the rate at which a cell evolves on the right branch  $\mathcal{R}_s$  is  $G_R(w, s)$ . For expansion, therefore, we need to show that  $|G_R(w, 0)| > |G_R(w, \sigma_A)|$ . We will, in fact, show that  $\frac{\partial}{\partial s} G_R(w, s) > 0$  for  $s \in [0, 1]$ . Since  $G_R(w, s) < 0$ , this gives the desired result.

Recall that  $G_R(w, s) \equiv g(\Phi_R(w, s), w)$ . Hence,  $\frac{\partial G_R}{\partial s} = \frac{\partial g}{\partial v} \frac{\partial \Phi_R}{\partial s}$ . From (2A.2),  $\frac{\partial g}{\partial v} < 0$ . To compute  $\frac{\partial \Phi_R}{\partial s}$ , note that

$$(3D.1) \quad F(\Phi_R(w, s), w, s) = 0$$

Differentiate this equation with respect to  $s$  to obtain

$$\frac{\partial \Phi_R}{\partial s} = -\frac{F_s}{F_v} = \frac{g_{syn}(\Phi_R(w, s) - v_{syn})}{F_v}$$

Now  $v - v_{syn} > 0$  because the synapse is inhibitory. Finally, we claim that  $F_v < 0$  near the left and right branches of the cubics. To see why this is true, differentiate (3D.1) with respect to  $w$ . This shows that

$$\frac{\partial \Phi_R}{\partial w} = -\frac{F_w}{F_v} = -\frac{f_w}{F_v}$$

We assumed in (2A.2) that  $f_w > 0$  near the singular solutions and we assumed above that  $\frac{\partial \Phi_R}{\partial w} > 0$ . It follows that  $F_v < 0$  and this completes the analysis.

### E. Remarks.

Our analysis has shown that an inhibitory network must have three properties in order to exhibit a stable periodic synchronous solution. The first is that cells must be able to escape the silent phase. We will assume throughout the remainder of the paper that each cell without coupling is excitable. In the example considered in this section, directly coupled excitable simple cells cannot give rise to oscillations. This is because the dimension of the slow manifold corresponding to each cell is only one: there is one slow intrinsic variable and there are no synaptic slow variables. In more complex networks, coupled excitable cells are able to escape the silent phase. This follows because there are at least two slow variables corresponding to each cell; one may be intrinsic and the other synaptic or both may be intrinsic slow variables. The higher dimensional slow manifold allows the excitable cells to escape the silent phase, although there is still a stable fixed point corresponding to the completely quiescent state.

The second requirement for stability of synchronous solutions is that the onset of inhibition must be sufficiently slow. (See also [3,11,32].) When one cell jumps up to the active phase, there must be a delay before inhibition is felt by the second cell. The second cell then has an opportunity to fire. The reason why these networks with direct synapses cannot synchronize is because the inhibition turns on the fast time scale; there is no such ‘window of opportunity.’

The third property is that there must be compression between the solutions corresponding to each cell as they evolve in phase space. This compression may take place as the cells evolve along higher dimensional slow manifolds or as they jump up or down between these manifolds. When discussing ‘compression,’ we will need to identify a metric in which the compression takes place. It will sometimes be convenient to use the usual Euclidean metric; however, it is often more convenient to use a time metric as was done earlier in this section, as well as in [20,32,35].

## 4. Mutually Coupled Complex Cells With Fast Inhibitory Synapses.

### A. Singular Solutions.

We now demonstrate that two mutually coupled complex cells, which are separately excitable, can exhibit stable synchronized oscillations when connected with fast inhibitory coupling. The synchronous solution may exist if the synapses are direct, but as in the previous section it can be stable only if the synapses are indirect. We assume that each

cell is excitable for fixed levels of input. As before, we analyze the network by constructing singular solutions. These consist of various pieces; each piece corresponds to a solution of either fast or slow equations. The fast equations are obtained by simply letting  $\epsilon = 0$  in (2B.1) and either (2B.2) or (2B.3). The slow equations are obtained by setting  $\tau = \epsilon t$  and then letting  $\epsilon = 0$ . Hence, if the synapses are direct, then the slow equations are

$$\begin{aligned}
 0 &= f(v_i, w_i, y_i) - g_{syn} s_j (v_i - v_{syn}) \\
 \dot{w}_i &= g(v_i, w_i) \\
 \dot{y}_i &= h(v_i, y_i) \\
 0 &= \alpha(1 - s_i)H(v_i - \theta_{syn}) - \beta s_i
 \end{aligned}
 \tag{4A.1}$$

One can reduce this system to equations for just the slow variables  $(y_i, w_i)$ . There are several cases to consider depending on whether both cells are silent, both are active or one is silent and the other is active. Here we derive the reduced slow equations for when the synapses are direct. The equations for indirect synapses are similar but there are more cases to consider.

We assume that the solution of the first equation in (4A.1) defines a cubic-shaped surface  $\mathcal{C}_s$  and the left and right branches of this surface can be expressed as  $v_i = \Phi_L(w_i, y_i, s_i)$  and  $v_i = \Phi_R(w_i, y_i, s_i)$ , respectively.

If both cells are silent, then each  $v_i < \theta_{syn}$  and  $s_i = 0$ . Let  $G_L(w, y, s) \equiv g(\Phi_L(w, y, s), w)$  and  $H_L(w, y, s) \equiv h(\Phi_L(w, y, s), y)$ . Then each  $(w_i, y_i)$  satisfies the equations

$$\begin{aligned}
 \dot{w} &= G_L(w, y, 0) \\
 \dot{y} &= H_L(w, y, 0)
 \end{aligned}
 \tag{4A.2}$$

If both cells are active, then each  $v_i > \theta_{syn}$  and the last equation in (4A.1) implies that  $s_i = \sigma_A \equiv \alpha/(\alpha + \beta)$ . Let  $G_R(w, y, s) \equiv g(\Phi_R(w, y, s), w)$  and  $H_R(w, y, s) \equiv h(\Phi_R(w, y, s), y)$ . Then each  $(w_i, y_i)$  satisfies the equations

$$\begin{aligned}
 \dot{w} &= G_R(w, y, \sigma_A) \\
 \dot{y} &= H_R(w, y, \sigma_A)
 \end{aligned}
 \tag{4A.3}$$

Finally suppose that one cell, say cell 1, is silent and cell 2 is active. Then the slow variables satisfy the reduced equations

$$\begin{aligned}
 \dot{w}_1 &= G_L(w_1, y_1, \sigma_A) \\
 \dot{y}_1 &= H_L(w_1, y_1, \sigma_A) \\
 \dot{w}_2 &= G_R(w_2, y_2, 0) \\
 \dot{y}_2 &= H_R(w_2, y_2, 0)
 \end{aligned}
 \tag{4A.4}$$

We may view a singular solution as two points moving around in the  $(y, w)$  slow phase space. Each point corresponds to one of the cells. The points evolve according to one of

the reduced slow systems until one of the points reaches a jump-up or jump-down curve. The cells then jump in the full phase space; however, the slow variables remain constant during the fast transitions. The points then ‘change directions’ in slow phase space and evolve according to some other reduced slow equations.

Since the cells are excitable, the reduced system (4A.2) with  $s = 0$  has a stable fixed point, which we denote by  $P_0$ . The slow phase space corresponding to (4A.2) is illustrated in Fig. 3A. Note that while some of the trajectories are attracted towards  $P_0$ , others are able to reach the jump-up curve. That is, even though the uncoupled cells are excitable, it is possible for a cell to begin in the silent phase and still fire. This will be important in the next section when we discuss the existence of the synchronous solution.

The following Lemma characterizes the left and right folds (or jump-up and jump-down curves) of  $\mathcal{C}_s$ . We assume here that  $f_y > 0$  on the left branch of  $\mathcal{C}_s$  while  $f_y < 0$  on the right. This assumption is justified, based on biophysical considerations, in Remark A1 of Appendix A.

**Lemma 1:** The left and right folds of  $\mathcal{C}_s$  can be expressed as  $J_L = \{(v_L(y, s), w_L(y, s), y)\}$  and  $J_R = \{(v_R(y, s), w_R(y, s), y)\}$  where  $\frac{\partial w_L}{\partial y} < 0$ ,  $\frac{\partial w_L}{\partial s} > 0$ ,  $\frac{\partial w_R}{\partial y} > 0$ , and  $\frac{\partial w_R}{\partial s} > 0$ .

**Proof:** Since  $v_L(y, s) = \Phi_L(w_L(y, s), y, s)$ , it follows from (4A.1) and the definition of folds that

$$(4A.5) \quad \begin{aligned} 0 &= f(\Phi_L(w_L(y, s), y, s), w_L(y, s), y) - g_{syn}s(\Phi_L(w_L(y, s), y, s) - v_{syn}) \\ 0 &= f_v(\Phi_L(w_L(y, s), y, s), w_L(y, s), y) - g_{syn}s \end{aligned}$$

Differentiating the first equation in (4A.5) with respect to  $w$  and using the second equation, we obtain

$$0 = \frac{\partial f}{\partial w} \frac{\partial w_L}{\partial s} - g_{syn}(\Phi_L(w_L(y, s), y, s) - v_{syn})$$

Hence,

$$(4A.6) \quad \frac{\partial w_L}{\partial s} = \frac{g_{syn}(\Phi_L(w_L(y, s), y, s) - v_{syn})}{f_w}$$

The right hand side of this expression has a positive numerator because the coupling is inhibitory and a positive denominator from (2A.2), so  $\frac{\partial w_L}{\partial s} > 0$ . Analogously,  $\frac{\partial w_R}{\partial s} > 0$ .

Similarly, differentiating with respect to  $y$  in (4A.5) yields  $0 = \frac{\partial f}{\partial w} \frac{\partial w_L}{\partial y} + \frac{\partial f}{\partial y}$ , or  $\frac{\partial w_L}{\partial y} = -\frac{f_y}{f_w}$ , with  $f_y$  and  $f_w$  evaluated on  $J_L$ . Analogously,  $\frac{\partial w_R}{\partial y} = -\frac{f_y}{f_w}$ , with  $f_y, f_w$  evaluated on  $J_R$ . The above assumptions on  $f_y$ , together with (2A.2), yield the desired result.

**Remark 1:** In the thalamic networks of interest, the  $y$  current has a much smaller reversal potential and maximal conductance than the  $w$  current. When a cell is in the silent phase, the disparity between the strengths of these currents can be mitigated by the deactivation of the  $w$  current. When a cell is in the active phase, however, this implies that  $|f_y| \ll |f_w|$ , so  $|\frac{\partial w_R}{\partial y}|$  is quite small. (See Remark A2 in Appendix A.) Correspondingly, in  $(w, y)$  phase space, the jump-down curve  $J_R$  is nearly horizontal (see Fig. 3B).

## B. Existence of the Synchronous Solution.

Here we illustrate why it is possible for a synchronous solution to exist in a network of mutually coupled complex cells even when the individual cells are excitable. A numerically generated picture of such a solution, projected onto the slow variables  $(y, w)$ , is shown in Fig. 3B. The precise equations which this particular solution satisfies and the parameter values used numerically are given in Appendix A.

One constructs the singular synchronous solution as follows. We begin when the cells are in the silent phase just after they have jumped down. The slow variables then evolve according to (4A.2). If they are able to reach the jump-up curve, then they jump up according to the fast equations. While in the active phase, the slow variables satisfy (4A.3) until they reach the jump-down curve. They then jump down according to the fast equations, and this completes one cycle of the synchronous solution.

It is not clear how to choose the starting point  $(y_i(0), w_i(0))$  so that the singular orbit returns precisely to this point after one cycle. Note, however, that the variables  $y_i$  relax very close to  $y_i = 0$  during the active phase. If we suppose that  $y_i \approx 0$  at the jump-down point then the value of  $w_i$  is determined; that is, for the coupled cells,  $w_i \approx w_R(0, \sigma_A)$ . A straightforward fixed point argument shows that the synchronous solution will therefore exist if the solution of (4A.2) which begins at  $(y_i, w_i) = (0, w_R(0, \sigma_A))$  is able to reach the curve of jump-up points.

The reason why a synchronous solution can exist even when the uncoupled cells cannot oscillate is that the synchronous solution lies on a different cubic during the active phase than the uncoupled cells. For this reason, the synchronous jumps down along a different curve than the uncoupled cells. From Lemma 1, the jump-down curve  $J_R(\sigma_A)$  has larger values of  $w$  than the jump-down curve  $J_R(0)$ ; see Fig. 3B. It is therefore possible for the coupled cells to jump down to a point from which they are able to eventually escape the silent phase, although the uncoupled cells jump down to a point from which they cannot escape.

There is a nice biophysical interpretation for why coupled excitable cells may be able to oscillate. Recall that a complex cell is an example of a thalamocortical relay cell. (See Section 7 for a more detailed discussion.) Then  $w$  corresponds to the inactivation variable of the  $I_T$  current. A larger value of  $w$  means that this current is more deinactivated. This implies that if the cells jump down at a larger value of  $w$ , then it is easier for the cells to become sufficiently depolarized so they can reach threshold and fire.

The construction of the synchronous solution for indirect synapses is very similar. The only difference is that after the cells jump up or jump down, there is a delay until the inhibition either turns on or turns off. The cells switch their cubic surface while in the silent and active phases, assuming that the delay is shorter than the time that the cells spend in each of their silent and active phases. We will assume that this is the case throughout the remainder of this paper.

## C. Stability of the Synchronous Solutions.

We assume throughout this section that the synapses are indirect. As in Section 3E

this condition is necessary for the stability of the synchronous solution in mutually coupled networks. Indirect synapses provide a window of opportunity for both cells to jump up during the same cycle; however, one must still show that the cells are brought closer together, or compressed, as they evolve in phase space.

It is not at all obvious how to define ‘compression.’ We need to demonstrate that the cells are brought closer together; however, this requires that we have a notion of distance between the cells. There are several possible metrics; each of these metrics has certain advantages on different pieces of the solution. One obvious metric is the Euclidean distance between the points in phase space corresponding to the cells. As seen in Section 3, it is sometimes convenient to work with a time metric; however, this is only naturally defined if the cells evolve on a one-dimensional slow manifold. Here the slow manifolds are two dimensional. We will describe several mechanisms for compression, each corresponding to a different piece of the singular solution.

It will be necessary to make some assumptions on the evolution of the cells. In a more complete discussion, we would have to consider other cases. However, our goal here is simply to show that it is possible for the synchronous solution to be stable for some robust class of systems.

### i. The Jump Up

Suppose that cell 1 lies on the jump-up curve when  $\tau = 0$ . After cell 1 fires, there is a delay in the onset of inhibition. We assume that cell 2 begins in the silent phase so close to the jump-up curve that it fires before it feels this inhibition. Suppose that cell 2 fires when  $\tau = T_0$ .

We now need make some assumptions on the nonlinearities; these are all satisfied for the example described in Appendix A. Let  $(y^*, w^*)$  be the point where the synchronous solution jumps up. We assume that

$$(A1) \quad G_L(y^*, w^*) < 0, \quad H_L(y^*, w^*) > 0, \quad G_R(y^*, w^*) < 0 \quad \text{and} \quad H_R(y^*, w^*) < 0$$

$$(A2) \quad |G_L(y^*, w^*, 0)| < |G_R(y^*, w^*, 0)| \quad \text{and} \quad |H_L(y^*, w^*, 0)| < |H_R(y^*, w^*, 0)|$$

Note that (A1) implies that  $w$  decreases and  $y$  increases in the silent phase just before the jump up while both  $w$  and  $y$  decrease in the active phase just after the jump up. (A2) implies that the  $w$  and  $y$  coordinates of both cells change at a faster rate after the jump up than before the jump up.

There are now several cases to consider depending on the orientation of the cells both before and after they jump up. We will only work out two of these in detail. These are the cases which arise most often for the system described in Appendix A. Similar analysis applies to the other cases.

Assume that  $w_1(0) < w_2(0)$ ,  $w_1(0) < w_2(T_0)$  and  $y_1(T_0) > y_2(0)$ . See Fig. 4A. These assumptions imply that  $|y_1(T_0) - y_2(T_0)| < |y_1(0) - y_2(0)|$  so there is compression in the  $y$ -coordinates after the jumps. From (A2), there is also compression in a time metric corresponding to the  $y$ -coordinate. For each  $\tau_0$ , let  $\rho_y(\tau_0)$  be the time it takes for cell 2 to evolve from its position at  $\tau = \tau_0$  until its  $y$ -coordinate is that of cell 1 when  $\tau = \tau_0$ . It

then follows that  $\rho_y(T_0) < \rho_y(0)$ .

We now show that there is also a compression in the time metric corresponding to the  $w$ -coordinate. This is denoted by  $\rho_w(\tau)$ . Let  $a^- = |G_L(y^*, w^*, 0)|$  and  $a^+ = |G_R(y^*, w^*, 0)|$ . Then

$$\begin{aligned}
 \rho_w(0) &\approx \frac{w_2(0) - w_1(0)}{a^-} = \frac{w_2(0) - w_2(T_0)}{a^-} + \frac{w_2(T_0) - w_1(0)}{a^-} \\
 &\approx T_0 + \frac{w_2(T_0) - w_1(0)}{a^-} > T_0 + \frac{w_2(T_0) - w_1(0)}{a^+} \\
 (4D.1) \quad &\approx \frac{w_1(0) - w_1(T_0)}{a^+} + \frac{w_2(T_0) - w_1(0)}{a^+} \\
 &\approx \rho_w(T_0)
 \end{aligned}$$

Now suppose that  $w_1(0) < w_2(0)$ ,  $w_1(0) < w_2(T_0)$  and  $y_1(T_0) < y_2(0)$ . The exact same calculation given in (4D.1) shows that there is compression in the time metric  $\rho_w$  across the jump up. A simple calculation also shows that there is compression in  $\rho_y$ .

## ii. The Active Phase

Next assume that the cells are active with  $x_i > \theta_x$ . Then each  $(y_i, w_i)$  satisfies (4A.3). It is easy to see why the cells are compressed in the Euclidean metric if we make some simplifying assumptions concerning the nonlinear functions  $g$  and  $h$ . These assumptions arise naturally if one considers the network in Appendix A; it is also a simple matter to extend this analysis to more general systems.

Suppose that  $g$  and  $h$  are of the form  $g(v, w) = (w_\infty(v) - w)/\tau_w(v)$  and  $h(v, y) = (y_\infty(v) - y)/\tau_y(v)$ . Note that while in the active phase,  $y_\infty(v)$  and  $w_\infty(v)$  are very small. Moreover,  $\tau_y(v)$  and  $\tau_w(v)$  are nearly constant. We assume here that while in the active phase,  $g(v, w) = -w/\tau_w$  and  $h(v, y) = -y/\tau_y$  where  $\tau_w$  and  $\tau_y$  are positive constants. It follows that each  $(w_i, y_i)$  satisfies the simple linear equations

$$\begin{aligned}
 \dot{w} &= -w/\tau_w \\
 \dot{y} &= -y/\tau_y
 \end{aligned}$$

If we ignore the jump-down curve, then each slow variable decays to 0 at an exponential rate. In particular, the distance between the cells decays exponentially. Actually, more is true: Each  $(y_i, w_i)$  approaches the origin tangent to the weakest eigendirection.

Now suppose that the jump-down curve passes close to the origin. The Euclidean distance between the cells still decreases exponentially and both cells jump down at nearly the same point. This is the point where the jump-down curve crosses the weakest eigendirection.

We note that there is another, more subtle, source of compression while the cells are active. There will be some period of time when cell 2 receives inhibition but cell 1 does not; that is,  $s_1 = \sigma_A$  but  $s_2 = 0$ . During this time, the  $(y_i, w_i)$  satisfy different equations. It is then possible that the trajectories  $(y_i(\tau), w_i(\tau))$  cross in the slow phase space. This leads

to a reversal of orientation between the cells as shown in Fig. 4B. In the next section, we will discuss why a reversal of orientation can lead to compression in the cells' trajectories.

### iii. The Jump Down

We now show that if the cells reverse their orientation while in the active phase, then this can lead to a form of compression after the cells jump down. Let  $T_i$  be the time when cell  $i$  jumps down. Recall that cell 1 jumped up first with  $w_1(0) < w_2(0)$ . We will assume that  $w_1(\tau) < w_2(\tau)$  as long both cells are active. Moreover, from Remark 1, the jump-down curve is nearly horizontal. Hence, cell 1 jumps down first; that is,  $T_1 < T_2$ .

If the cells' trajectories cross while in the active phase, then  $y_1(T_1) < y_2(T_2)$ . This is shown in Fig. 4B. Let  $\rho_y^A(T_1)$  be the time it would take for the solution of (4A.3) starting at  $(y_2(T_1), w_2(T_1))$  to reach the  $y$ -coordinate  $y_1(T_1)$ . It follows that  $\rho_y^A(T_1) > T_2 - T_1$ .

For  $T_1 < \tau < T_2$ , cell 1 evolves in the silent phase with  $y$  increasing while cell 2 evolves in the active phase with  $y$  decreasing. If  $y_1(T_2) < y_2(T_2)$ , then  $|y_2(T_2) - y_1(T_2)| < |y_2(T_1) - y_1(T_1)|$  so there is compression in the  $y$ -coordinates of the cells across the jump. Now suppose that  $y_1(T_2) > y_2(T_2)$  as shown in Fig. 4B. Let  $\rho_y^S(T_2)$  be the time it would take for the solution of (4A.2) starting at  $(y_2(T_2), w_2(T_2))$  to reach the  $y$ -coordinate of cell 1. Since  $y_2(T_1) > y_1(T_1)$ , it follows that  $\rho_y^S(T_2) < T_2 - T_1$ . We have now demonstrated that  $\rho_y^S(T_2) < T_2 - T_1 < \rho_y^A(T_1)$ . That is, there is compression in the time metric corresponding to the  $y$ -coordinate. We note that since the jump-down curve is nearly horizontal, any compression in the  $w$ -coordinates is, to first order, neutral.

A numerical example of orientation reversal in two cells' trajectories in  $(y, w)$ -space is shown in Fig. 4C. At the top of the Figure, the cells are in the silent phase. Each cell jumps up where the corresponding  $y'_i = 0$ ; chronologically, cell 1 jumps up first. In the active phase, the trajectories cross, because the cells experience different levels of inhibition; cell 2 receives inhibition first. The paths cross again at the bottom left of the Figure after the leading cell, cell 1, falls down to the silent phase.

### iv. The Silent Phase

Suppose that both cells lie in the silent phase with  $x_i < \theta_{syn}$ . Then each  $(y_i, w_i)$  satisfies (4A.2) until one of them reaches the jump-up curve. We now define a metric between the cells and, in Appendix B, we analyze how to choose parameters to guarantee that the metric decreases as the cells evolve in the silent phase. This metric is similar to that introduced in [32].

Suppose that cell 1 reaches the jump-up curve first and this is at the point  $(y_1^*, w_1^*)$ . (See Fig. 12 in Appendix B.) Fix some time  $\tau_0$  and let  $w_L^{\tau_0}$  be the physical translate of the jump-up curve to the position of cell 1 at time  $\tau_0$ ; that is,  $(y_1^*, w_1^*)$  is translated to the point  $(y_1(\tau_0), w_1(\tau_0))$ . Then the 'distance' between  $(y_1(\tau_0), w_1(\tau_0))$  and  $(y_2(\tau_0), w_2(\tau_0))$  is the time it takes for the solution of (4A.2) which begins at  $(y_2(\tau_0), w_2(\tau_0))$  to cross  $w_L^{\tau_0}$ . This is certainly well defined as long as the two cells are sufficiently close to each other.

One can compute explicitly how this metric changes as the cells evolve in the silent

phase. The computation is rather technical so we present this in Appendix B. A more complete discussion of how this metric is used to prove the stability of the synchronous solution of two mutually coupled simple cells with slow synapses is given in [32].

#### D. Further Remarks.

The analysis in this section is similar to that in [32], where it was proven that two mutually coupled simple cells with slow inhibitory coupling can synchronize. In both papers, two slow variables are needed to achieve both the existence and the stability of the synchronous solution. The additional dimension to the branch of the slow manifold corresponding to the silent phase allows excitable cells to escape. The compression of cells can take place as the cells evolve along the higher dimensional slow manifold or as they jump up or down. The compression during the jumping process depends on the geometry (or slope) of the curve of knees and the orientation of the cells both before and after the jumps. Parameters which determine this slope may, therefore, have subtle effects on the stability of the synchronous solution;  $g_{syn}$  is one such parameter [see (4A.6)]. The results in [32] provide precise conditions on combinations of parameters which ensure that the synchronous solution is stable. Increasing  $g_{syn}$ , for example, may sometimes stabilize the synchronous solution; however, when other parameters satisfy a different relationship, increasing  $g_{syn}$  may destabilize the synchronous solution.

The size of the domain of attraction of the synchronous solution is, to a large extent, determined by the delay in the onset of inhibition. The two cells are able to fire together if the trailing cell lies within the window of opportunity determined by this delay. If the trailing cell lies outside of this window, then the network typically exhibits antiphase behavior in which the cells take turns firing, although other network behavior is possible. The system may ‘crash,’ for example, since the completely quiescent state is asymptotically stable.

In our analysis, we assumed that the cells and coupling are homogeneous. The effect of heterogeneities on mutually coupled simple cells with slow synapses was studied in [3,12,46]. They found that the synchronous solution is not very robust to mild levels of heterogeneities; a 5% variation in parameters was sufficient to destroy synchronous behavior. We have done a number of numerical simulations in order to study the effects of heterogeneities on the network considered in this section. Our numerical results are consistent with those in previous studies.

## 5. Globally Inhibitory Networks With Simple Cells.

### A. Introduction.

We now consider the network described in Section 2C. Recall that in this network,  $E$ -cells excite  $J$ -cells, which in turn inhibit  $E$ -cells. We assume, for now, that there are just two  $E$ -cells, denoted by  $E_1$  and  $E_2$ , and there is one  $J$ -cell, which we denote as  $J$ . Larger networks are considered later. Each cell is assumed to be a simple cell; the  $E$ -cells are identical to each other, but they may be different from the  $J$ . Each cell is also assumed to be excitable for fixed levels of input.

The system of equations corresponding to each  $E_i$  is

$$(5A.1) \quad \begin{aligned} v'_i &= f(v_i, w_i) - g_{inh} s_J (v_i - v_{inh}) \\ w'_i &= \epsilon g(v_i, w_i) \\ s'_i &= \alpha(1 - s_i) H(v_i - \theta) - \beta s_i \end{aligned}$$

while the equation for  $J$  is

$$(5A.2) \quad \begin{aligned} v'_J &= f_J(v_J, w_J) - \frac{1}{2}(s_1 + s_2) g_{exc}(v_J - v_{exc}) \\ w'_J &= \epsilon g_J(v_J, w_J) \\ s'_J &= \alpha_J(1 - s_J) H(v_J - \theta_J) - \epsilon K_J s_J \end{aligned}$$

Here, each synapse is direct. Indirect synapses will be needed when we discuss the stability of solutions. Note that the inhibitory variable  $s_J$  turns off on the slow time scale. The reason why we write the equations this way will become clear in the analysis. We assume that  $\beta = O(1)$ ; however, there is no problem in extending the analysis if  $\beta = O(\epsilon)$ . If  $v_i > \theta$ , then  $s_i \rightarrow \sigma_A \equiv \frac{\alpha}{\alpha + \beta}$  on the fast time scale.

Two types of network behavior are shown in Figs. 8 and 9. A synchronous solution, in which each cell fires during every cycle, is shown in Fig. 9. In Fig. 8, each excitatory cell fires every second cycle, while  $J$  fires during every cycle. This type of solution will be referred to as a clustered solution. In the next section, we will construct singular orbits corresponding to each of these solutions and then analyze their stability. The constructions will help determine conditions for when the different solutions exist and are stable. As we shall see, these constructions carry over to larger networks.

## B. The Synchronous Solution.

We now construct a singular trajectory corresponding to a synchronous solution in phase space. Again, the trajectory for each cell lies on the left or right branch of a cubic nullcline during the silent and active phases. Which cubic a cell inhabits depends on the total synaptic input that the cell receives. Nullclines for the  $E_i$  are shown in Fig. 5A and those for  $J$  in Fig 5B. Note in Fig. 5A that the  $s_J = 1$  nullcline lies above the  $s_J = 0$  nullcline, while in Fig. 5B, the  $s_{tot} \equiv \frac{1}{2}(s_1 + s_2) = \sigma_A$  nullcline lies below the  $s_{tot} = 0$  nullcline. This is because the  $E_i$  receive inhibition from  $J$  while  $J$  receives excitation from the  $E_i$ . We will make several assumptions concerning the flow in the following construction. These are justified later.

We begin with each cell in the active phase just after it has jumped up. These are the points labeled  $P_0$  and  $Q_0$  in Fig. 5. Each  $E_i$  evolves down the right branch of the  $s_J = 1$  cubic, since the synapses are direct, while  $J$  evolves down the right branch of the  $s_{tot} = \sigma_A$  cubic. We assume that the  $E_i$  have a shorter active phase than  $J$  so each  $E_i$  reaches the right knee  $P_1$  and jumps down to the point  $P_2$  before  $J$  jumps down. We also assume that at this time  $J$  lies above the right knee of the  $s_{tot} = 0$  cubic.  $J$  must then jump from the point  $Q_1$  to the point  $Q_2$  along the  $s_{tot} = 0$  cubic. On the next piece of the solution,  $J$  moves down the right branch of the  $s_{tot} = 0$  cubic while the  $E_i$  move up the left branch of

the  $s_J = 1$  cubic. When  $J$  reaches the right knee  $Q_3$  it jumps down to the point  $Q_4$  along the left branch of the  $s_{tot} = 0$  cubic. Since  $s_J$  turns off on the slow time scale, the  $E_i$  do not jump to another cubic.

Now the inhibition to  $E_i$  turns off slowly. The trajectory for  $E_i$  moves upwards, with increasing  $w_i$ , until it crosses the  $w$  nullcline. Then each  $w_i$  starts to decrease. If this orbit is able to reach a left knee, then it jumps up to the active phase and this completes one cycle of the synchronous solution. When  $E_i$  jumps up,  $J$  also jumps up if it lies above the left knee of the  $s_{tot} = \sigma_A$  cubic.

We now derive more quantitative conditions for when the singular synchronous solution exists. It is not at all obvious, for example, why we needed to assume that the active phase of  $J$  is longer than that for the  $E_i$ . It is also not clear what conditions are needed to assure that the  $E_i$  are able to reach a jump-up curve once they are released from inhibition. These two issues are actually closely related.

We first discuss how the  $E_i$  can reach the jump-up curve. For this, it is convenient to derive equations for the evolution of the slow variables  $(w_i, s_J)$  as was done in Section 4A. Let  $\tau = \epsilon t$ , denote the left branch of the cubic  $f(v, w) - g_{inh}s(v - v_{inh}) = 0$  by  $v = \Phi_L(w, s)$  and let  $G_L(w, s) \equiv g(\Phi_L(w, s), s)$ . Then each  $(w_i, s_J)$  satisfies the slow equations

$$(5B.1) \quad \begin{aligned} \dot{w} &= G_L(w, s_J) \\ \dot{s}_J &= -K_J s_J \end{aligned}$$

The phase plane corresponding to this system is illustrated in Fig. 6. There are two important curves shown in the Figure. The first is the jump-up curve  $w = w_L(s_J)$ ; this is the curve of ‘left knees.’ The second curve, which is denoted by  $W_F(s_J)$ , corresponds to the fixed points of first two equations in (5A.1) in which the input  $s_J$  is held constant. This corresponds to the  $w$ -nullcline of (5B.1).

We need to determine when a solution  $(w(\tau), s_J(\tau))$  of (5B.1) beginning with  $s_J(0) = 1$  and  $w(0) < W_F(1)$  can reach the jump-up curve  $w_L(s_J)$ . This is clearly impossible if  $W_F(1) < w_L(0)$  so we shall assume that  $W_F(1) > w_L(0)$ . If  $w(0) > w_L(0)$  and  $K_J$  is sufficiently large, then the solution will certainly reach the jump-up curve; this is because the solution will be nearly vertical as shown in Fig. 6. If, on the other hand,  $K_J$  is too small, then the solution will never be able to reach the jump-up curve. This is because the solution will slowly approach the curve  $W_F(s_J)$  and lie very close to this curve as  $s_J$  approaches zero. This is also shown in Fig. 6. We conclude that the cells are able to escape the silent phase if the inhibitory synapses turn off sufficiently quickly and the  $w$ -value of the cells are sufficiently large when this deactivation begins. Escape is not possible for very slowly deactivating synapses. A biophysical interpretation of this is that escape is possible for  $GABA_A$  synapses and will occur if the cell’s  $I_T$  current is sufficiently deinactivated when inhibition begins to wear off.

We assume that  $K_J$  is large enough so that escape is possible. Choose  $W_{esc}$  so that the solution of (5B.1) that begins with  $s_J(0) = 1$  will be able to reach the jump-up curve only if  $w(0) > W_{esc}$ . The existence of the singular synchronous solution now depends on

whether the  $E_i$  lie in the region where  $w_i > W_{esc}$  when  $J$  jumps down to the silent phase. We claim that this requires that the active phase of  $J$  be sufficiently long. One can give a simple estimate on how long this active phase must be as follows.

Suppose that all the cells jump up when  $\tau = 0$ , the  $E_i$  jump down when  $\tau = \tau_E$  and  $J$  jumps down when  $\tau = \tau_J$ . We require that  $w_i(\tau_J) > W_{esc}$ . Since the time the  $E_i$  spend in the silent phase before they are released from inhibition is  $\tau_J - \tau_E$ , this implies that  $\tau_J - \tau_E$  must be sufficiently large. Hence,  $J$ 's active phase must be sufficiently longer than the  $E_i$ 's. More precisely, let  $w_{RK}$  be the value of  $w$  at the right knee of the  $s_J = 1$  cubic and let  $\tau_L$  be the time it takes for the solution of the first equation in (5B.1) with  $s_J = 1$  to go from  $w = w_{RK}$  to  $w = W_{esc}$ . We require that

$$(5B.2) \quad \tau_J - \tau_E > \tau_L$$

**Remark 2:** In the previous construction we assumed that the synaptic inhibition  $s_J$  decays on the slow time scale. This was needed to insure that  $J$  recovers sufficiently in its silent phase so it can fire once excited by the cells  $E_i$ . In particular,  $J$  can fire only if  $(w_J, s_{tot})$  lies above the left knee of the  $s_{tot} = 1$  cubic. Hence, if the recovery of  $J$  is rather fast, then one can allow  $s_J$  to turn off rather quickly; that is,  $K_J$  can be chosen to be quite large. This will be important in the next section when we consider the stability of the synchronous solution, as these parameters help determine its domain of attraction.

### C. Stability of the Singular Synchronous Solution.

We now demonstrate that the synchronous solution is stable if the synapse  $s_J$  is indirect and the active phase of  $J$  is sufficiently long. We start with the  $E_i$  a small distance apart, just after they have both jumped up to the active phase. Assume that this causes  $J$  to fire. We will show that after one cycle, both of the  $E_i$  are so close that they must fire together again. Moreover, there is a contraction in the distance between the  $E$ -cells during each cycle.

The analysis proceeds as in the previous section. We assume that the active phases of the  $E_i$  are shorter than that of  $J$  so that the  $E_i$  return to the silent phase and proceed up the left branch of the  $s_J = 1$  cubic before  $J$  jumps down. As the  $E_i$  move up this left branch, they approach the point  $P_L$  where the  $s_J = 1$  cubic intersects the  $w$ -nullcline. See Fig. 5A. If the active phase of  $J$  is sufficiently long, then the  $E_i$  lie as close as we please to  $P_L$ , and therefore to each other, when  $J$  jumps down. This is precisely what is required to guarantee that they will both fire together during the next cycle. While in the silent phase, the  $E_i$  approach  $P_L$  at an exponential rate (in the slow time scale). This leads to a very strong compression of Euclidean distance between the cells while in the silent phase. This compression is certainly stronger than any possible expansion over the remainder of the cycle. After the  $J$ -cell falls down,  $s_J$  decays on the slow time scale. This allows the  $J$ -cell to recover, so that it can fire when excited by the firing of the  $E$ -cells and the whole cycle repeats.

We need to assume that  $s_J$  corresponds to an indirect synapse for the same reason as we did previously. When one of the  $E$ -cells fires, this causes  $J$  to fire, which, in turn, sends

inhibition back to the other  $E$ -cell. If  $s_J$  is direct, then this causes the second  $E$ -cell to be ‘stepped on’ on the fast time scale and the synchronous solution cannot be stable. Note that the time between the firings of the  $E$ -cells is determined by  $K_J$ , the rate at which  $s_J$  decays. If  $K_J$  is large, then the time between firings is short; it is then easier for the second cell to pass through the ‘window of opportunity’ provided by the indirect synapse.

Our analysis has shown that the dynamics of the  $J$ -cell can influence the domain of attraction of the synchronous solution in several ways. If  $J$ ’s active phase is long, then the  $E$ -cells lie close to each other, near  $P_L$ , when  $J$  jumps down and releases them from inhibition. Moreover, if  $J$  recovers quickly in the silent phase, then  $K_J$  can be chosen to be large, as noted in Remark 2. Both of these factors make it easier for the  $E$ -cells to pass through window of opportunity and fire during the same cycle. Hence, they both enhance the domain of attraction of the synchronous solution.

**Remark 3:** There are important differences between the ways in which mutually coupled and globally inhibitory networks use inhibition to synchronize oscillations. In mutually coupled networks, a second slow variable is required for the existence of the synchronized solution; it allows the cells to escape from the silent phase. The second slow variable is also required for the compression of the cells as they evolve in phase space. The existence and stability of the synchronous solution in globally inhibitory networks, on the other hand, is controlled by the dynamics of the  $J$ -cell. If the  $J$ -cell’s active phase is long enough, then this pushes the  $E$ -cells, in their silent phase, to a position from which they can escape; moreover, this provides a strong compression of the  $E$ -cells. For this network, we still require that the inhibition decays on the slow time scale; however, the reason is so that the  $J$ -cell can recover sufficiently. The slow recovery is not needed to allow the  $E$ -cells to escape or for compression. In fact, the domain of stability of the synchronous solution is increased if the synapses decay quickly. Once the  $E$ -cells are released from inhibition, they must all pass through the window of opportunity. A fast decay of inhibition allows them to pass through this window that much quicker.

#### D. Clustered Solution.

We now describe the geometric construction of the singular antiphase, or clustered, solution. It suffices to consider one-half of a complete cycle. During this half-cycle,  $E_1$  fires and returns to the initial position of  $E_2$ ,  $J$  fires and returns to its initial position, and  $E_2$  evolves in the silent phase to the initial position of  $E_1$ . By symmetry, we can then continue the solution for another half-cycle with the roles of  $E_1$  and  $E_2$  reversed.

When  $E_1$  jumps up, it forces  $J$  to jump up to the right branch of the  $s_{tot} = \frac{1}{2}\sigma_A$  cubic. Then  $E_1$  moves down the right branch of the  $s_J = 1$  cubic, while  $J$  moves down the right branch of the  $s_{tot} = \frac{1}{2}\sigma_A$  cubic and  $E_2$  moves up the left branch of the  $s_J = 1$  cubic. We assume, as before, that  $E_1$ ’s active phase is shorter than  $J$ ’s active phase, so  $E_1$  jumps down before  $J$  does so. It is possible that  $J$  lies below the right knee of the  $s_{tot} = 0$  cubic at this time, in which case  $J$  also jumps down. If  $J$  lies above this right knee, then it moves down the right branch of the  $s_{tot} = 0$  cubic until it reaches the right knee and then jumps down. During this time, both  $E_1$  and  $E_2$  move up the left branch of the  $s_J = 1$  cubic.

After  $J$  jumps down,  $s_J(\tau)$  slowly decreases. If  $E_2$  is able to reach the jump-up curve,

then it fires and this completes the first half cycle of the singular solution. Suppose that  $\tau = \tau_F$  when this occurs. For this to be one-half of an antiphase solution, we need that  $w_2(\tau_F) = w_1(0)$ ,  $w_1(\tau_F) = w_2(0)$ , and  $w_J(\tau_F) = w_J(0)$ . We now derive conditions for when the antiphase solution exists. These will imply that the active phase of  $J$  cannot be too long or too short, compared with the active phase of the  $E_i$ . If  $J$ 's active phase is too long, then the network exhibits synchronous behavior as described before. If  $J$ 's active phase is too short, then the system approaches the stable quiescent state.

Suppose that  $E_1$  and  $J$  jump up when  $\tau = 0$ ,  $E_1$  jumps down when  $\tau = \tau_E$ , and  $J$  jumps down when  $\tau = \tau_J$ . Let  $\tau_L$ ,  $\tau_{esc}$ , and  $W_{esc}$  be as defined in the previous section. To have a clustered solution, we require that

$$(5D.1) \quad w_1(\tau_J) < W_{esc} < w_2(\tau_J)$$

The second inequality is necessary to allow  $E_2$  to fire during the second half cycle. The first inequality guarantees that  $E_1$  does not fire during this half cycle. It follows from the definitions that the first inequality is equivalent to

$$(5D.2) \quad \tau_J - \tau_E < \tau_{esc}$$

Next we derive a similar expression for the second inequality in (5D.1). For  $w_0 < w_1$ , let  $\rho(w_0, w_1)$  to be the time it takes for a solution of the first equation in (5B.1) with  $s_J = 1$  to go from  $w_0$  to  $w_1$ . We need to prove that  $\rho(w_{RK}, w_2(\tau_J)) > \tau_{esc}$ . Now,

$$\rho(w_{RK}, w_2(\tau_J)) = \rho(w_{RK}, w_2(0)) + \rho(w_2(0), w_2(\tau_J))$$

Moreover,  $w_{RK} = w_1(\tau_E)$  and  $w_2(0) = w_1(\tau_F)$ . Hence,

$$\rho(w_{RK}, w_2(\tau_J)) = \rho(w_1(\tau_E), w_1(\tau_F)) + \rho(w_2(0), w_2(\tau_J))$$

Clearly,  $\rho(w_2(0), w_2(\tau_J)) = \tau_J$ , because  $E_2$  lies on the  $s_J = 1$  cubic for  $0 < \tau < \tau_J$ . It is not true that  $E_1$  lies on the  $s_J = 1$  cubic for  $\tau_E < \tau < \tau_F$ ; however, if the first equation in (5B.1) is weakly dependent on  $s_J$ , then we have that  $\rho(w_1(\tau_E), w_1(\tau_F)) \approx \tau_F - \tau_E$ . In this case, the second inequality in (5D.1) is equivalent to

$$(5D.3) \quad \tau_F - \tau_E + \tau_J > \tau_{esc}$$

Recall that it is sometimes possible to choose the parameter  $K_J$  to be rather large; see Remark 2. In this case,  $\tau_F - \tau_J$  is small; that is,  $E_2$  escapes the silent phase as soon as it is released from inhibition. Then (5D.3) is approximately equivalent to

$$(5D.4) \quad \tau_J > \frac{1}{2}(\tau_E + \tau_{esc})$$

Combining (5D.2) and (5D.4) leads to the following condition for the existence of a clustered solution if the synaptic variable  $s_J$  turns off quickly:

$$(5D.5) \quad \frac{1}{2}(\tau_E + \tau_{esc}) < \tau_J < \tau_E + \tau_{esc}$$

### E. Further Remarks.

The geometric constructions of the synchronous and clustered solutions extend in a straightforward manner to globally inhibitory networks with an arbitrary number of excitatory cells  $E_i$ . Of course, in a larger network there are more possibilities for clustered solutions; however, if each cluster contains (approximately) the same number of cells, then inequalities similar to (5D.5) must be satisfied. This is similar to analysis in [35] where precise conditions are derived for the existence of clustered states in a locally excitatory and globally inhibitory network model for scene segmentation.

The synchronous and clustered solutions are quite robust to heterogeneities and changes of parameters. The synchronous solution is considerably more robust for this network than it was for the mutually coupled networks considered in Section 3 and in [32]. This is because the global inhibitor  $J$  provides a powerful compression mechanism. The strength of this compression depends to a large extent on how long  $J$  remains active and this is controlled by intrinsic properties of  $J$ . While  $J$  is active, all the  $E$ -cells approach the same fixed point at an exponential rate. They are then ready to jump up together when released from inhibition. There is no such powerful compression mechanism for the mutually coupled networks.

## 6. Globally Inhibitory Networks with Complex Cells.

The discussion in the previous section generalizes to globally inhibitory networks with complex cells. The primary difference is that each cell contains an additional slow variable, so it is necessary to consider a higher dimensional slow phase space. Here we outline the geometric construction of the singular synchronous solution. Of course, this solution exists only if certain assumptions are made on the nonlinear functions in the model. We describe necessary assumptions as they arise in the discussion. In the next section, we demonstrate numerically that these assumptions are satisfied for the model of the spindle sleep rhythm.

We begin by considering the network in Section 2C in which there are two  $E$ -cells and one  $J$ -cell. Each  $E$ -cell is assumed to be a complex cell and without any coupling satisfies equations of the form (2A.3). We assume, for now, that  $J$  is a simple cell; this will simplify the discussion somewhat. Later we discuss how to generalize the construction when  $J$  evolves via more complex dynamics. Assume, for now, that the synapses are direct. Then each  $E_i$  satisfies a system of the form:

$$\begin{aligned}
 v'_i &= f(v_i, w_i, y_i) - g_{inh} s_J (v_i - v_{inh}) \\
 w'_i &= \epsilon g(v_i, w_i) \\
 y'_i &= \epsilon h(v_i, y_i) \\
 s'_i &= \alpha(1 - s_i)H(v_i - \theta) - \beta s_i
 \end{aligned}
 \tag{6.1}$$

The inhibitory cell satisfies (5A.2).

During the silent and active phases, each  $E$ -cell lies on either the left or right branch of one of the cubic surfaces  $\{(v, w, y) : f(v, w, y) - g_{inh} s_J (v - v_{inh}) = 0\}$ . We write these branches as  $\{v = \Phi_\alpha(w, y, s_J)\}$  where  $\alpha = L$  or  $R$ . Let  $G_\alpha(w, y, s_J) \equiv g(\Phi_\alpha(w, y, s_J), w)$  and  $H_\alpha(w, y, s_J) \equiv h(\Phi_\alpha(w, y, s_J), y)$ . The cubic surface on which the  $E$ -cells lie depends

on the value of  $s_J$ ; moreover, the evolution of  $s_J$  depends on whether the  $J$ -cell is active or silent. If  $J$  is silent ( $v_J < \theta_J$ ) then the slow variables corresponding to the  $E$ -cells satisfy the equations

$$(6.2) \quad \begin{aligned} \dot{w} &= G_\alpha(w, y, s_J) \\ \dot{y} &= H_\alpha(w, y, s_J) \\ \dot{s}_J &= -K_J s_J \end{aligned}$$

where  $\alpha = L$  or  $R$ , depending on whether the  $E$ -cell is silent or active. If  $J$  is active ( $v_J > \theta_J$ ) then the slow variables evolve according to the equations

$$(6.3) \quad \begin{aligned} \dot{w} &= G_\alpha(w, y, 1) \\ \dot{y} &= H_\alpha(w, y, 1) \end{aligned}$$

The slow variables satisfy these systems until either one of the  $(w_i, y_i, s_J)$  reaches a fold of a cubic surface or the  $J$ -cell jumps up or down. The set of folds forms two surfaces of knees. These surfaces can be written as  $\{w = w_\alpha(y, s_J)\}$ ,  $\alpha = L$  or  $R$ , where  $w_\alpha(y, s_J)$  is as in Lemma 1.

Fig. 7 illustrates the evolution of the slow variables  $(w_i, y_i, s_J)$  for the singular synchronous solution. We begin at the point labeled  $P_1$  on the jump-up surface  $w = w_L(y, s_J)$ . The  $E$ -cells then jump up and this forces  $J$  to jump up. Hence,  $s_J \rightarrow 1$ . This corresponds to the segment in Fig. 7 that connects  $P_1$  to the point  $P_2$  on the  $s_J = 1$  surface. Each cell then evolves in the active phase with  $s_J = 1$  and each  $(w_i, y_i)$  satisfies (6.3) with  $\alpha = R$ . As before, we assume that the active phases of the  $E$ -cells are shorter than that of  $J$ . Hence, the  $E$ -cells jump down when the  $(w_i, y_i)$  reach the jump-down curve  $w_i = w_R(y_i, 1)$ . This is at the point labeled  $P_3$  in Fig. 7. While  $J$  lies in the active phase, the  $(w_i, y_i)$  satisfy (6.3) with  $\alpha = L$ . At  $P_4$ ,  $J$  jumps down and the  $(w_i, y_i, s_J)$  satisfy (6.2) with  $\alpha = L$  until they reach the jump-up curve. This then completes one cycle of the singular solution.

The stability analysis proceeds just as in the previous section. What is crucial for stability is that  $J$  remains active long enough. The  $E$ -cells must then approach the stable fixed point of (6.3), with  $\alpha = L$ , on the left branch of the  $s_J = 1$  surface. This provides the compression needed for stability.

The construction of a clustered solution is also very similar to that described in the previous section. We do not describe the construction here; some comments are given in the next section. Similar analysis also holds if the  $J$ -cell satisfies more complex dynamics. What is important here is that  $J$ 's active phase is sufficiently long in comparison with the active phase of the  $E$ -cells. This is discussed in detail in the next section when we consider the influence of biophysical parameters on models for the spindle sleep rhythm.

## 7. Thalamic Network.

### A. Introduction.

The model for the spindle sleep rhythm falls into the framework of the network considered in the preceding section. The two populations of cells in the model both lie in

the thalamus. These are the thalamocortical relay (TC) cells and the thalamic reticularis (RE) cells, corresponding to the  $E$ -cells and  $J$ -cells, respectively. One difference between the spindle model and those considered earlier is that the spindle model contains numerous RE, as well as TC, cells. The RE cells communicate with each other through fast inhibitory synapses, as illustrated in the network shown in Section 2C.

During a spindle pocket, the network exhibits behavior similar to the clustered solution discussed in the previous section. The RE population is synchronized while the TC cells break up into groups; cells within each group are synchronized while cells within different groups are desynchronized. The network also exhibits completely synchronized rhythms. The synchronized rhythms arise, for example, when fast inhibition is removed from the network. Recent results have also shown that the synchrony can arise if the RE population receives additional excitation, corresponding to cortical input. Hence, the network can transform from clustering to synchronized behavior without any change in the inhibitory synapses. We will explain the dynamic mechanisms responsible for these rhythms and transitions between them, using the geometric approach.

## B. Model.

The following model contains many parameters and nonlinear functions. These are given in Appendix A. The cells are modeled using the Hodgkin-Huxley formalism [17]; the equations are very similar to those in [15].

The equations of each TC-cell are:

$$(7B.1) \quad \begin{aligned} v_i' &= -I_T(v_i, h_i) - I_{sag}(v_i, r_i) - I_L(v_i) - I_A - I_B \\ h_i' &= (h_\infty(v_i) - h_i)/\tau_h(v_i) \\ r_i' &= (r_\infty(v_i) - r_i)/\tau_r(v_i) \end{aligned}$$

Note that this is a complex cell, with  $h_i$  and  $r_i$  corresponding to  $w$  and  $y$  respectively. The terms  $I_T$ ,  $I_{sag}$ , and  $I_L$  are intrinsic currents; they are given by:  $I_T(v, h) = g_{Ca}m_\infty^2(v)h(v - v_{Ca})$ ,  $I_{sag}(v, r) = g_{sag}r(v - v_{sag})$  and  $I_L(v) = g_L(v - v_L)$ . The terms  $I_A$  and  $I_B$  represent the fast and slow inhibitory input from the RE-cells. We model the fast inhibition  $I_A$  as in previous sections; that is,  $I_A = g_A(v_i - v_A)\frac{1}{N_{TR}}\sum s_A^j$  where  $g_A$  and  $v_A$  are the maximal conductance and the reversal potential of the synaptic current. The sum is over all RE-cells which send input to this TC-cell and  $N_{TR}$  represents the maximum number of RE cells which send inhibition to a single TC cell. Each synaptic variable  $s_A^j$  satisfies the first order equation

$$(7B.2) \quad s_A^{j'} = \alpha_R(1 - s_A^j)H(v_R^j - \theta_R) - \beta_R s_A^j$$

where  $v_R^j$  is the membrane potential variable of the  $j^{th}$  RE-cell. Motivated by recent experiments [7,8], we model the slow inhibition  $I_B$  somewhat differently from before. We first discuss, however, the model for the RE-cells.

The equations of each RE-cell are:

$$\begin{aligned}
(7B.3) \quad v_R^i{}' &= -I_{RT}(v_R^i, h_R^i) - I_{AHP}(v_R^i, m_i) - I_{RL}(v_R^i) - I_{RA} - I_E \\
h_R^i{}' &= (h_{R\infty}(v_R^i) - h_R^i) / \tau_{Rh}(v_R^i) \\
m_i{}' &= \mu_1[Ca]_i(1 - m_i) - \mu_2 m_i \\
[Ca]_i{}' &= -\nu I_{RT} - \gamma[Ca]_i
\end{aligned}$$

The  $I_{RT}$ ,  $I_{AHP}$ , and  $I_{RL}$  represent intrinsic currents. These are given by  $I_{RT}(v, h) = g_{Ca}^R m_{R\infty}^2(v) h(v - v_{Ca}^R)$ ,  $I_{AHP}(v, m) = g_{AHP} m(v - v_K)$  and  $I_{RL}(v) = g_{RL}(v - v_{RL})$ . More details concerning the biophysical significance of each term are given in [15,33].

In (7B.3),  $I_{RA}$  represents the inhibitory input from other RE-cells. It is modeled as  $I_{RA} = g_{RA}(v_R^i - v_{RA}) \frac{1}{N_{RR}} \sum s_{RA}^j$  where the sum is over all RE-cells which send input to the  $i^{th}$  RE-cell. Each synaptic variable  $s_{RA}^j$  satisfies a first order equation similar to (7B.2). The term  $I_E$  represents excitatory input from the TC-cells and is expressed as  $I_E = g_E(v_R^i - v_E) \frac{1}{N_{RT}} \sum s_E^j$  where the sum is over all TC-cells which send excitatory input to the  $i^{th}$  RE cell. The synaptic variables  $s_E^j$  also satisfy first order equations similar to (7B.2).

It remains to discuss how we model the slow inhibitory current  $I_B$ . Similarly to [7], we assume that

$$I_B = g_B \frac{s_{bi}^4}{s_{bi}^4 + \lambda} (v_i - v_B)$$

where  $s_{bi}$ , along with variable  $x_{bi}$ , satisfies

$$\begin{aligned}
(7B.4) \quad s_{bi}' &= k_1 H(x_{bi} - \theta_{xb})(1 - s_{bi}) - k_2 s_{bi} \\
x_{bi}' &= \frac{k_3}{N_{TR}} \left[ \sum H(v_R^i - \theta_{Rb}) \right] (1 - x_{bi}) - k_4 x_{bi}
\end{aligned}$$

The parameters are such that  $x_{bi}$  can only become activated if a sufficiently large number of RE-cells have their membrane potentials  $v_R^i$  above the threshold  $\theta_{Rb}$ . The threshold is chosen rather large so the RE bursts must be sufficiently powerful to activate  $x_{bi}$ . Once  $x_{bi}$  becomes activated it turns on the synaptic variable  $s_{bi}$ ; the expression  $s_{bi}^4$  in  $I_B$  further delays the effect of the inhibition on the postsynaptic cell.

### C. Numerical Simulations.

A clustered solution is shown in Fig. 8. There are 3 RE cells in this example and they oscillate in synchrony at about 12.5 Hz; one of the RE cells is shown in Fig. 8A. The RE cells synchronize due to excitation from the TC population. This is discussed in more detail later (see Section 7D). There are 6 TC cells and they form two clusters, each oscillating at half of the RE oscillation frequency, as shown in Fig. 8B. In Fig. 8C, we show the time courses of the fast ( $s_A$ ) and slow ( $s_b$ ) inhibitory synaptic variables, respectively. Note that the fast inhibition activates during every cycle. This provides the hyperpolarizing current needed to deactivate each TC cell's  $I_T$  current. The fast inhibition is also needed to

desynchronize the TC cells so they can form clusters. The slow current  $I_B$  never activates during this solution. This is because the RE cells do not fire powerful enough bursts; that is, the membrane potentials  $v_R^i$  do not rise above the threshold  $\theta_{Rb} = -25mV$  long enough to activate the variables  $x_{bi}$ .

A synchronous solution is shown in Fig. 9. The parameters are exactly as in Fig. 8 except we set  $g_{RA} = 0$ ; that is, we have turned off the fast inhibition between RE cells. Note in Fig. 9 that each TC cell fires during every cycle along with the RE cells. The slow inhibitory current  $I_B$  now activates during every cycle. Comparing the slow inhibitory variable with the fast inhibitory variable in Fig. 9C, we see that the slow inhibition stays on longer and that it both turns on and turns off more gradually. Removing the RE-TC fast inhibition as well ( $g_A = 0$ ) enhances  $s_b$  activation and TC synchronization. Geometric analysis is very useful in understanding why removing fast inhibition allows slow inhibition to activate and why this, in turn, leads to synchronization of the network. This is discussed in the next subsection.

In Fig. 10 we plot the trajectory  $(h_i(\tau), r_i(\tau), s_b(\tau))$  corresponding to the synchronous solution shown in Fig. 9. We also plot the numerically computed surface of knees corresponding to the jump-up points; there is a similar jump-down surface, but it is not shown. The behavior of the trajectory is consistent with that discussed in the previous section. For example, the cells jump up when the trajectory crosses the jump-up surface of knees (approximately, since  $\epsilon \neq 0$  numerically). In Fig. 11 we show a similar plot but for the clustered solution shown in Fig. 8. Here we use  $s_A(\tau)$  instead of  $s_b(\tau)$ . The trajectory is more complicated since two clusters fire instead of just one.

Our numerical studies show that the synchronous and clustered solutions are robust to moderate levels of heterogeneities and variations in the parameters. For example, these solutions were not affected by heterogeneities of about 20% in sag conductances and about 5% in the TC  $I_T$  conductance. Stronger TC heterogeneities tend to promote TC clustering in this model. In the resultant patterns, TC cells with similar properties fire together, independent of the way they are initially perturbed from synchrony.

Since the length of the RE cell active phase is crucially important in determining whether the TC cells will synchronize or cluster, variations in RE intrinsic properties may have important consequences for the network behavior. Weakening the  $I_{AHP}$  or  $I_L$  conductances or strengthening  $I_T$  tend to lengthen the RE active phase by making  $v_R'$  less negative there. Corresponding changes in reversal potentials have a similar effect. Modulating these parameters may, therefore, switch the network rhythm between synchrony and clustering.

## D. Remarks.

### i. Removing Fast Inhibition.

Fast inhibition occurs in two places: the RE cells inhibit themselves as well as the TC cells. Removing fast inhibition has different consequences for each of these synaptic connections and both of these help to synchronize the TC cells [8,15]. Removing the RE-TC fast inhibition is clearly helpful for synchronization among the TC cells since the fast inhibition has a very short rise time. Note that the fast inhibitory synapses are direct in

(7B.1), (7B.2). This rise time helps determine the domain of attraction of the synchronous solution; a short rise time corresponds to a small domain of attraction. In fact, it is precisely this inhibition that is responsible for desynchronizing the TC cells during the clustered solution.

Removing the RE-RE fast inhibition is perhaps even more crucial for synchronizing the TC cells. This allows the RE cells to fire longer, more powerful bursts which, in turn, activate the slow inhibitory current  $I_B$ . The analysis in previous sections demonstrates that long, powerful bursting of the RE cells is a necessary condition for the TC cells to synchronize. Our numerical simulations (e.g. Figs. 8-11) show, in fact, that the TC cells will synchronize even if fast inhibition is removed from within the RE population but not from the RE-TC connections.

Why removal of inhibition leads to stronger RE bursts can be easily understood by considering trajectories in phase space. This removal forces the RE cells to lie on the right branch of a different cubic while in the active phase. If the RE cells are simple, then the cubic of the disinhibited cells lies below the cubic of the cells with inhibition. The disinhibited cells therefore jump up to larger values of membrane potential; moreover, their jump-down point (right knee) lies below the jump down point of the inhibited cells. The disinhibited RE cells, therefore, have a longer active phase. Similar analysis holds if the RE cells are complex.

Note that the slow inhibitory current  $I_B$  has slower rise and decay times than  $I_A$ . The slow rise time enhances the domain of attraction of the synchronous solution. The slow decay time can help to bring the cells closer together while in the silent phase, as discussed in Section 4. Hence, both effects enhance the ability of the TC cells to synchronize.

## ii. Role of the Sag Current.

We view the TC cells as examples of complex cells. If one removes the sag current  $I_h$ , or keeps it constant, then they become simple cells. Hence, questions concerning the differences between networks with simple or complex cells are closely related to issues related to the role of the sag current. The analysis in Sections 3 and 4 shows that in mutually coupled networks, whether the cells are simple or complex is significant. Added complexity allows the cells to escape from the silent phase and also leads to possible compression mechanisms. In globally inhibitory networks, however, there does not seem to be that much of a difference in network behavior if the cells are simple or complex. The dynamical mechanisms responsible for the synchronous and clustered solutions are basically the same for simple or complex cells. We do not view the sag current, therefore, as playing a direct role in the generation of these rhythms. Recall that oscillations arise when the cells are capable of escaping from the silent phase. The sag current helps modulate the intrinsic properties of the TC cells and this can, in turn, determine whether or not escape is even possible. From a more biophysical viewpoint, the sag current depolarizes the TC cells while they are silent. Hence, a stronger sag current raises the TC's resting potential. If this resting potential is too large, then inhibitory input from the RE cells may not be capable of hyperpolarizing the TC cells sufficiently to deactivate the  $I_T$  current. If this is the case, then the TC cells will not be able to fire (i.e. escape the silent phase).

This relates closely to some theories about mechanisms responsible for the waxing and waning behavior during the spindle rhythm [1,5,16]. It is known that the sag current is modulated by many substances that shift its activation curve, providing a different amount of this current at each particular voltage level. To incorporate waxing and waning, we follow [5] and assume that the sag conductance depends on calcium as well as on voltage. Calcium slowly increases while the TC cells oscillate; this increases the sag conductance, which slowly depolarizes the cells. This eventually prevents deinactivation of  $I_T$ , which stops the spindle oscillations. A new spindle pocket forms when enough of the calcium has been removed by extrusion or uptake to allow oscillations to start again. The new spindle pocket may be initiated by input from cortical cells which oscillate at a very slow rhythm. This is discussed in more detail in the next subsection.

We note that increasing the sag current (within the range where escape is possible) tends to enhance the TC synchronization, and this also decreases the amplitude and period of TC bursts. The enhancement of synchronization occurs because the increased sag current tends to depolarize the TC cells more rapidly; it was shown in the previous section that this leads to stronger compression. The decrease in amplitude and period occurs because increasing the sag conductance lowers the left branch of the cubic corresponding to the TC cells while in the silent phase but raises the right branch of the cubic while the cells are in the active phase. This is because the current is depolarizing while the cells silent but hyperpolarizing while the cells are active. Increasing  $g_{sag}$  also makes the slope of the curve of knees of the silent phase more negative; this allows TC cells to jump up to the active phase at smaller values of  $h_i$  and  $r_i$ , further decreasing the amplitude and period of oscillation.

### iii. Synchronization Among the RE Cells.

The RE cells are synchronized during the spindle rhythm. This is primarily due to the excitation they receive from the TC cells. While only about half of the TC cells fire during each cycle, if each TC cell sends excitation to several RE cells, then every RE cell will receive a sufficient amount of excitation to fire during every cycle.

Experiments have also shown that the RE cells can sustain synchronized rhythms when these cells are completely isolated [30]. In fact, these are the experiments which motivated many of the theoretical studies concerning how synchronization can arise in a population of inhibitory cells. If one considers the RE cells to be modeled as simple cells, then the conclusion of these studies is that synchronization is possible only if the decay of inhibition is sufficiently slow. However, modeling the RE cells as in (7B.3), we consider them to be complex cells; the slow variables are  $h_R^i$  and  $m_i$ . We then conclude that synchronization is possible even if the inhibition decays quickly.

### iv. Cortical Inputs.

Cortical inputs are believed to be important in the generation of the spindle and delta sleep rhythms [4,8,28,31]. During these rhythms, cortical cells oscillate at a slow rhythm of about .1-.2 Hz. This slow rhythm organizes the spindle pockets, as was discussed earlier. A new spindle pocket is initiated when cortical cells fire and send excitation to the RE

cells. The RE cells fire and send inhibition to the TC cells, eventually causing them to fire in clusters.

Recent papers have also emphasized the importance of the cortex in the generation of spike-and-wave epileptic oscillations [8,29,31]. Some experiments have suggested that this can arise without removing fast inhibition in the thalamus [8,31]. Recall that in the mechanism discussed previously, disinhibition of the RE cells leads to more powerful RE bursts and this permits the TC cells to synchronize. If one does not remove the fast inhibition among the RE cells, but instead induces excitation from the cortex, then this will have the same effect: the RE cells will fire more powerful bursts because of the additional excitation (their cubics are lowered). Hence, the TC cells can synchronize even though they receive fast inhibition from the RE cells.

During the delta sleep rhythm, the RE cells fire at the frequency of, and phase-locked to, the slow cortical rhythm. The TC population rhythm is very regular at 1-4 Hz. Each TC cell fires a number of times and then has subthreshold oscillations for a number of cycles. The TC cells are periodically revived within the frequency range of the slow rhythm. A mechanism is proposed in [33] for the transition between the spindle and delta rhythms. Since fast inhibition tends to force the TC cells to cluster during spindling and the TC cells are synchronized during delta, this effect of fast inhibition must be removed during the delta rhythm. It was shown in [33] that in order to remove this effect, it is not necessary to actually change any parameters associated with the fast inhibitory synapses. Instead, it suffices to hyperpolarize the RE cells; this can be accomplished, for example, by increasing their leak conductance. This makes the RE cells insensitive to excitation from the TC cells. Since the RE cells do not respond to cycle by cycle excitation from the TC cells, they are functionally absent from the network and are unable to send fast inhibition back to the TC cells. The RE cells do respond, however, to the cortical cells by firing at the slow rhythm. During the resulting cycle, the TC cells receive both fast and slow inhibition, which cause them all to fire. The continuing presence of slow inhibition allows the TC cells to fire for a few more cycles and also helps them to synchronize.

Our analysis has shown that it is possible for the TC to synchronize even in the presence of fast inhibition if the RE cell bursts are powerful enough. This does not, however, contradict the argument in [33] that the effect of fast inhibition to the TC cells must be removed during delta. Since the RE cells fire at the slow rhythm in delta, their bursts are completely absent (after the first cycle) while the TC cells fire. Hence, the RE cells do not produce the powerful bursts that would be needed to synchronize the TC cells if the effect of the fast inhibition remained.

## **v. Variations in Synchronous Oscillations.**

The thalamic network may exhibit other types of solutions than those discussed above. This is because assumptions required for the geometric constructions of the solutions may not be satisfied for some ranges of parameter values. Subtle variations in network behavior can arise as parameters that change the underlying geometry of phase space are varied.

One possibility that appears, for certain biophysically relevant parameter values, is that the right knees of each RE-cell's family of cubics lie above the left knees of the RE-cell's

cubics. In this case, each RE cell recovers instantly upon jump-down. Hence, synchrony is possible even if the inhibition to the TC cells decays on the fast time scale, since slow decay of inhibition was only needed to allow the RE cells to recover. It is important to note that our requirement of a long RE cell active phase for stable synchrony can still be met here. To see this, note that the RE cubics are extremely flat in the active phase (that is, for relevant  $v_R$  values,  $h_R$  changes little along them) and lie near the  $h_R = 0$  axis. When an RE cell is excited and fires, its  $v_R$  jumps up to a large value on the fast time scale. Its  $v_R$  then decreases on the slow time scale. This slow decrease occurs because  $h_R$  and the synaptic excitation variable  $s_E$  (see Appendix A and note that  $\beta_E$  is small) decay slowly. This can yield a sufficiently long RE active phase for stable synchrony (with nearly constant  $h_R$  throughout the oscillation).

In this scenario, if the TC cells approach sufficiently close to the stable equilibrium in the silent phase while the RE cells are still active, then they can all fire as soon as they are disinhibited by RE jump-down. Hence, stable synchrony can occur here in the presence of fast inhibition even though the RE-TC fast inhibitory synapses are direct. The TC firing immediately excites the RE cells to fire again. If one or more TC cells have not crossed the middle branch of their  $v$ -nullclines when an RE cell's voltage reaches  $\theta_R$ , however, then those TC cells turn back and clusters form. Hence, the thresholds for inhibition and excitation influence the TC population behavior in this case.

One other subtlety to note, returning to the usual RE nullcline configuration, is that the firing of a single TC cell may be insufficient to induce RE firing. This is the case if an RE cell has not sufficiently recovered when the lead TC fires. Oscillations may nonetheless be sustained if the firing of following TC cells induces RE cell firing. Thus, the length of time for RE cell recovery should be measured up to the time when the last TC cell, not the lead TC cell, fires.

## 8. Discussion.

We have considered a series of networks in order to study how network components contribute to emergent population rhythms. This work is motivated by recent models for sleep rhythms; however, the analysis and methods are quite general, so they should apply to other models as well. Our results clarify the multiple roles inhibition can play in producing different rhythms. Which rhythms are produced depends on how the inhibition interacts with intrinsic properties of the cells; the nature of these interactions depends on the underlying architecture of the network.

Inhibition may help either to synchronize or to desynchronize oscillations, depending on several factors. Fast onset of inhibition tends to desynchronize the cells, because when one cell fires it then quickly 'steps on' other cells. For this reason, we generally need to assume that the synapses are indirect for stable synchronization to occur. Slow offset of inhibition may help to synchronize the oscillations; it can lead to compression of the cells while they evolve in either the silent or active phases. Compression (or expansion) can also take place as the cells jump up or down between the silent and active phases. This depends on the geometry of curves (or surfaces) of knees, which, in turn, depends on both the intrinsic and the synaptic components, such as  $g_{syn}$  and  $g_{sag}$ . Another source

of compression arises in the globally inhibitory networks. While the inhibitory cell  $J$  is active, it produces sustained inhibition to the  $E$ -cells. This forces the  $E$ -cells close to a stable fixed point and, therefore, close to each other. This can be a very powerful source of compression of the  $E$ -cells.

We have demonstrated that mutually coupled networks of excitable cells with indirect fast inhibitory coupling can produce synchronized rhythms. This is not possible if the network contains only simple cells. The geometric approach helps explain why the additional network complexity allows for synchronized rhythms. The additional complexity translates, within the framework of the geometric approach, to higher dimensional slow manifolds. This allows the cells to escape from the silent phase. It also leads to additional sources of compression. We conclude that synchronization is possible in mutually coupled inhibitory networks if there are at least two slow variables in the intrinsic and/or synaptic dynamics. This has relevance for isolated RE cell populations, which can synchronize even though they include fast inhibition.

By studying both mutually coupled and globally inhibitory networks we have seen how the underlying network architecture can influence the possible population rhythms. As discussed in Remark 3, these two networks use inhibition in very different ways to synchronize oscillations. In both networks, when one  $E$ -cell fires, it produces inhibition among the remaining  $E$ -cells. This is accomplished by a single connection in the mutually coupled networks, but through two connections via the inhibitory cell  $J$  in the globally inhibitory networks. The globally inhibitory networks are much more robust because the  $J$ -cell has its own internal dynamics and can, therefore, control the amount of inhibition it sends back to the  $E$ -cells. In mutually coupled networks, the inhibition is, in some sense, ‘slave’ to the dynamics of the  $E$ -cells.

Globally inhibitory networks can produce different rhythms depending on the intrinsic dynamics of the inhibitory  $J$ -cells. If the  $J$ -cells produce powerful bursts, then the resulting inhibition leads to synchronized rhythms. A rapid rate of synchronization, and a large domain of attraction for the synchronous solution, are achieved when the following factors are present: indirect synapses to provide a window of opportunity, a long  $J$ -cell active phase to enhance compression among  $E$ -cells, and a fast  $J$ -cell recovery coupled with relatively fast synaptic decay. Less powerful inhibition, or a smaller window of opportunity, results in clustering among the  $E$ -cells. The network crashes if the amount of inhibition is too small. In the models for sleep rhythms, there are several possible ways to control the RE cells’ bursts and therefore to control the emergent network behavior. More powerful RE bursts result from removal of fast inhibition from among the RE cells or from the addition of excitatory input from the cortex. Other intrinsic RE parameters, such as a leak conductance, may also greatly influence the RE cells’ dynamics. We have seen how such considerations help explain the transition between spindle, delta, and paroxysmal discharges in RE-TC networks.

The geometric approach helps to clarify the mechanisms, both biological and mathematical, responsible for the population rhythms. The analysis can lead to precise statements for when a rhythm is possible. For example, a TC cell can fire only if it is sufficiently hyperpolarized; this deinactivates the  $I_T$  current. A geometric interpretation of this is that

a TC cell can fire only if, during the silent phase, it lies in the region where trajectories are able to reach the jump-up curve of knees. By considering the slow equations corresponding to the TC cells [see (6.2)], one can then derive conditions for when a TC will fire. In this sense, the geometric analysis helps clarify how different parameters influence the rhythms. For example, the analysis demonstrates that the sag current plays different roles in generating synchronized rhythms in mutually coupled and globally inhibitory networks. In mutually coupled networks, fast inhibition cannot produce synchronized rhythms unless the cells are complex. If the cells are considered to be TC cells, then this implies that the sag current is essential for synchronization in the presence of fast inhibition; it provides an additional slow variable. In globally inhibitory networks, however, synchronization can arise even if the cells are simple. Hence, the sag current contributes to the rhythms by adjusting the intrinsic properties of the cells so that they are capable of oscillating at all.

We note that the geometric approach used here is somewhat different from that used in many dynamical systems studies. All of the networks considered here consist of many differential equations, especially for larger networks. Traditionally, one would interpret the solution of this system as a single trajectory evolving in a very large dimensional phase space. We consider several trajectories, one corresponding to each cell, moving around in a much lower dimensional phase space. After reducing the full system to a system for just the slow variables, the dimension of the lower dimensional phase space equals the number of slow intrinsic variables and slow synaptic variables corresponding to each cell. In the worst case considered here, there are two slow variables for each complex cell and one slow synaptic variable; hence, we never have to consider phase spaces with dimension more than three. Of course, the particular phase space we need to consider may change, depending on whether the cells are active or silent and also depending on the synaptic input that a cell receives.

Our analysis of globally inhibitory networks is closely related to that in [35,39,40], where a model for scene segmentation is considered. In that model, different clusters correspond to different objects in a visual scene; the phases of oscillators encode the binding of pixels with similar sensory features. The model (denoted as LEGION) there includes both local excitation and global inhibition. The global inhibitory cell satisfies a simple one dimensional differential equation. Because of its simple dynamics, the global inhibitor there cannot easily control the emergent network behavior via adjustments to its intrinsic properties. Using a more complex model for the global inhibitor in LEGION may have important consequences, particularly since there is often no unique answer to the question of how a given scene should be segmented. A house, for example, may be grouped into a single segment if viewed from afar. The same house, if viewed nearby, may be broken into multiple segments, including a door, a roof, windows, and other elements. The analysis in this paper demonstrates that the level of inhibition produced by the global inhibitor controls the level of synchrony among the  $E$ -cells. Hence, by controlling this level of inhibition, one can control the level of resolution that the LEGION network will produce.

*Acknowledgments.* Research for this paper was supported in part by the NSF grant DMS-9423796. Some of the research was done while the authors were visiting the IMA at the University of Minnesota.

## Appendix A.

The equations for the TC and RE cells in the thalamic network are given in Section 7B. As our biophysical mutually coupled network of complex cells, we considered a pair of TC cells, each governed by (7B.1); note that in the case of simple cells without slow inhibition, these could be thought of as simplified RE cells or TC cells. The synaptic variables in this model satisfy (2B.3). For numerical simulations, we approximated Heaviside functions by functions of the form

$$H_\infty(v) = \frac{1}{1 + \exp(-\kappa(v - \theta))}$$

The functions  $h_\infty(v)$ ,  $m_\infty(v)$ ,  $r_\infty(v)$ ,  $h_{R\infty}(v)$  and  $m_{R\infty}(v)$  are assumed to be of the same form, namely, if  $\xi = h, m, r, h_R$  or  $m_R$ , then

$$\xi_\infty(v) = \frac{1}{1 + \exp((v + \theta_\xi)/\sigma_\xi)}$$

Further, we take

$$\tau_h(v) = \tau_{h0} + \frac{\tau_{h1}}{1 + \exp((v + v_{\tau h})/\sigma_{\tau h})}$$

with  $\tau_{Rh}(v)$  having an analogous form, and

$$\tau_r(v) = \tau_{r0} + \frac{\tau_{r1}}{\exp((v + v_{\tau r0})/\sigma_{\tau r0}) + \exp(-(v + v_{\tau r1})/\sigma_{\tau r1})}$$

To generate our numerical figures, we started cells under a slight perturbation from a synchronous state. For Figures 3B and 4C, we used the following parameter values, based on [15,33].  $I_T : g_{Ca} = 2.5, \theta_m = 57.0, \sigma_m = -6.0, v_{Ca} = 140.0, \theta_h = 81.0, \sigma_h = 4.0, \tau_{h0} = 10.0, \tau_{h1} = 73.\bar{3}, v_{\tau h} = 78.0, \sigma_{\tau h} = 3.0$ ;  $I_{sag} : g_{sag} = 0.2, v_{sag} = -50.0, \theta_r = 75.0, \sigma_r = 5.5, \tau_{r0} = 20.0, \tau_{r1} = 1000.0, v_{\tau r0} = 71.5, \sigma_{\tau r0} = 14.2, v_{\tau r1} = 89.0, \sigma_{\tau r1} = 11.6$ ;  $I_L : g_L = 0.025, v_L = -75.0$ ;  $I_A : g_A = 0.4, v_A = -79.0, \alpha = 16.0, \beta = 4.0, \theta_x = 0.1, \kappa = 100.0, \epsilon\alpha_x = 0.3, \epsilon\beta_x = 0.1, \theta_{syn} = -50.0$ . We did not include slow inhibition here.

To generate the clustered solution displayed in Figures 8 and 11, we used the following parameter values, also based on [15,33]. Six TC cells:  $I_T : g_{Ca} = 1.5, \theta_m = 59.0, \sigma_m = -9.0, v_{Ca} = 90.0, \theta_h = 82.0, \sigma_h = 5.0, \tau_{h0} = 66.\bar{6}, \tau_{h1} = 333.\bar{3}, v_{\tau h} = 78.0, \sigma_{\tau h} = 1.5$ ;  $I_{sag} : g_{sag} = 0.15, v_{sag} = -40.0, \theta_r = 75.0, \sigma_r = 5.5, \tau_{r0} = 20.0, \tau_{r1} = 1000.0, v_{\tau r0} = 71.5, \sigma_{\tau r0} = 14.2, v_{\tau r1} = 89.0, \sigma_{\tau r1} = 11.6$ ;  $I_L : g_L = 0.2, v_L = -76.0$ ;  $I_A : g_A = 0.1, v_A = -84.0, \alpha = 8.0, \beta = 0.05, \theta_R = -50.0, \kappa_A = 2.0$ ;  $I_B : g_B = 0.05, v_B = 95.0, \lambda = 10^{-4}, k_1 = 0.1, k_2 = 0.05, \theta_{xb} = 0.8, \kappa_{xb} = 0.02, k_3 = 0.5, k_4 = 0.005, \theta_{Rb} = -25.0, \kappa_b = 2.0$ . Three RE cells:  $I_{RT} : g_{Ca}^R = 2.0, \theta_m^R = 52.0, \sigma_m^R = -9.0, v_{Ca}^R = 90.0, \theta_h^R = 72.0, \sigma_h^R = 2.0, \tau_{h0}^R = 66.\bar{6}, \tau_{h1}^R = 333.\bar{3}, v_{\tau h}^R = 78.0, \sigma_{\tau h}^R = 1.0$ ;  $I_{AHP} : g_{AHP} = 0.1, v_K = -90.0, \mu_1 = 0.02, \mu_2 = 0.025, \nu = 0.01, \gamma = 0.08$ ;  $I_{RL} : g_{RL} = 0.3, v_{RL} = -76.0$ ;  $I_{RA} : g_{RA} = 0.25, v_{RA} = -84.0$ , other parameters as in  $I_A$  for the TC cells;  $I_E : g_E = 0.6, v_E = 0, \alpha_E = 2.0, \beta_E = 0.05, \theta_E = -35.0, \kappa_E = 2.0$ . [Note that in the current  $I_E$ , the variables  $s_E^j$  satisfy an equation of the form (7B.2), with the parameters  $\alpha_E, \dots$  replacing  $\alpha_R, \dots$ .]

To generate the synchronous solution displayed in Figures 9 and 10, we used the same parameter values except  $\alpha = 16, \beta = 0.2, \sigma_{\tau h} = 3.0, \sigma_{\tau h}^R = 2.0, g_{RA} = 0$ . By setting

$g_{RA} = 0$ , we removed the RE-RE fast inhibition; for  $\alpha = 16, \beta = 0.2$  with the same initial conditions and  $g_{RA} = 0.25$ , the solution forms two clusters but slow inhibition is slightly activated and it eventually destabilizes, while for  $g_{RA} = 0.5$ , the solution forms two clusters without activation of slow inhibition.

**Remark A1:** We assumed in the proof of Lemma 1 that for complex cells,  $f_y > 0$  in the silent phase, while  $f_y < 0$  in the active phase. This is justified for the TC-cell model for the following reason. Note that  $y$  corresponds to the variable  $r$ ; hence,  $f_y = -g_{sag}(v - v_{sag})$ . Since  $v_{sag} \approx -40mV$  typically, while  $v$  ranges from around  $-80mV$  in the silent phase to at least  $-30mV$  in the active phase, the result follows.

**Remark A2:** We claimed in Remark 1 that  $|\frac{\partial w_R}{\partial y}|$  is quite small. This is also shown numerically in Fig. 3B. We can understand analytically why this is so by recalling from the proof of Lemma 1, that  $\frac{\partial w_\alpha}{\partial y} = -\frac{f_y}{f_w}$  for  $\alpha = L$  or  $R$  corresponding to the silent or active phase respectively. From (7B.1),

$$(A1) \quad \frac{\partial w_\alpha}{\partial y} = -\frac{g_{sag}(v - v_{sag})}{g_{Ca}m_\infty^2(v)(v - v_{Ca})}$$

Typical values are  $g_{sag} \approx .04$  up to  $2.0$ ,  $v_{sag} \approx -40mV$ ,  $g_{Ca} \approx 2.5$ ,  $v_{Ca} \approx 140mV$ . In the silent phase,  $m_\infty(v)$  is small, so the numerator and denominator in (A1) have similar magnitudes, even though  $v \approx -80mV$ . In the active phase, however,  $m_\infty(v) \approx 1$  while  $v \approx 0$ , typically. Hence,  $|\frac{\partial w_R}{\partial y}|$  is quite small.

## Appendix B.

Consider a pair of complex cells in the active phase, with mutual inhibitory coupling. Suppose that the cells are perturbed from synchrony such that the lead cell falls down to the silent phase at time  $\tau_1$  and the following cell falls down at time  $\tau_2 > \tau_1$ . During the silent phase, for  $\tau \geq \tau_2$ , the slow dynamics of the two cells are given by

$$(B1) \quad \begin{aligned} w' &= g(v, w) \\ y' &= h(v, y) \\ s' &= -Ks \end{aligned}$$

where  $v$  satisfies  $v = \Phi_L(w, y, s)$  and  $' = \frac{d}{d\tau}$ . Let  $V(\tau) = (g(w, v), h(y, v), -Ks)$ . The equation of variations that describes the evolution of tangent vectors to the flow of (B1) is

$$(B2) \quad \begin{aligned} \delta w' &= -a^w \delta w - b^w \delta y - c^w \delta s \\ \delta y' &= -a^y \delta w - b^y \delta y - c^y \delta s \\ \delta s' &= -K \delta s \end{aligned}$$

where  $a^w = -\partial g / \partial w$ ,  $b^w = -\partial g / \partial y = -\partial g / \partial v \cdot \partial \Phi_L / \partial y$ , and so on.

Fix the cell which jumps up out of the silent phase first as cell 1 and call the other cell 2. Let  $T_i$  denote the jump-up time of cell  $i$  and restrict to  $\tau \in [\tau_2, T_1]$ . Let  $(\eta(\tau), \rho(\tau), \sigma(\tau))$

denote the vector from the position of cell 1 to that of cell 2, such that  $(\eta, \rho, \sigma)$  satisfies (B2); see Fig. 12 for a two-dimensional representation of this set-up.

Next, let  $w_L(y, s)$  denote the projection of the left surface of knees to  $(w, y, s)$ -space and let  $(a, b, c) = \nabla[w_L(y_1(T_1), s(T_1)) - w(T_1)] = (-1, \frac{\partial w_L}{\partial y}(y_1(T_1), s(T_1)), \frac{\partial w_L}{\partial s}(y_1(T_1), s(T_1)))$ . Let  $w_L^\tau$  denote the physical translate of  $w_L(y, s)$  along the path of cell 1 to the position of cell 1 at time  $\tau$ ; for example, at time  $\tau_2$ , cell 1 lies in  $w_L^{\tau_2}$ . Again, see Fig. 12.

We define the time  $T(\tau)$  as the time for cell 2 to flow to its first intersection with  $w_L^\tau$ . This satisfies

$$(B3) \quad (a, b, c) \cdot [(\eta, \rho, \sigma) + \int_0^{T(\tau)} V(\tau + \xi) d\xi] = 0$$

where  $V$  is evaluated along the path of cell 2 (Fig. 12), but

$$(B4) \quad \int_0^{T(\tau)} V(\tau + \xi) d\xi = \int_0^{T(\tau)} (V(\tau) + \xi V'(\tau) + O(\xi^2)) d\xi = V(\tau)T(\tau) + O(T^2)$$

For small perturbations from synchrony, if the vector field of (B1) is  $O(1)$ , then the  $O(T^2)$  term in (B4) can be neglected. Substituting the approximation (B4) into (B3) yields, at leading order,

$$(B5) \quad T(\tau) = -\frac{(a, b, c) \cdot (\eta, \rho, \sigma)}{(a, b, c) \cdot V} = \frac{\eta - b\rho - c\sigma}{-g(w_2, v_2) + bh(y_2, v_2) - cKs_2}$$

since  $a = -1$ . Henceforth, we omit the arguments indicating evaluation along the path of cell 2 when this is clear.

A sufficient condition for compression in the silent phase is that  $T'(\tau) < 0$  for  $\tau \in [\tau_2, T_1]$ . Thus, we proceed to compute  $T'(\tau)$ . Since  $(\eta, \rho, \sigma)$  and  $V(\tau)$  satisfy (B2), we differentiate, substitute from (B2), and simplify to obtain

$$(B6) \quad T'(\tau) = \frac{[V(\tau) \times (\eta, \rho, \sigma)] \cdot [(a, b, c) \cdot DV] \times (a, b, c)^\dagger}{((a, b, c) \cdot V(\tau)^T)^2}$$

where  $\dagger$  denotes transpose.

Geometrically, the determinant of three vectors gives the volume of the parallelepiped they bound. The numerator of  $T'(\tau)$  consists of such a determinant, with the three edges of the parallelepiped given by the vector field, the vector from the position of cell 1 to that of cell 2, and a third vector. This last vector relates the linearization of the vector field to the gradient of the translate of the surface of knees.

Next, consider

$$(B7) \quad \begin{aligned} Z &\equiv (Z_1, Z_2, Z_3) := V \times (\eta, \rho, \sigma) \\ &= (\sigma h + \rho K s, -\sigma g - \eta K s, \rho g - \eta h) \\ &= ((h, -Ks) \wedge (\rho, \sigma), (\eta, \sigma) \wedge (g, -Ks), (g, h) \wedge (\eta, \rho)) \end{aligned}$$

Differentiating (B7) and using (B2) gives, in system form,

$$(B8) \quad \begin{aligned} Z_1' &= -(b^y + K)Z_1 + a^y Z_2 \\ Z_2' &= b^w Z_1 - (a^w + K)Z_2 \\ Z_3' &= c^w Z_1 + c^y Z_2 - (a^w + b^y)Z_3 \end{aligned}$$

For simple cells, without the current  $y$ , (B6) simplifies to

$$T'(\tau) = \frac{\sigma g + \eta K s}{(g + cKs)^2} (c(a^w - K) + c^w) = \frac{-Z_2}{(g + cKs)^2} (c(a^w - K) + c^w)$$

Moreover,  $Z_1 \equiv 0$ , so  $Z_2' = -(a^w + K)Z_2$ . Hence, the sign of  $Z_2(\tau)$  is invariant for  $\tau \in [\tau_2, T_1]$ . In [32],  $Z_2(\tau_2) = (w_1(\tau_2) - w_2(\tau_2))Ks_2(\tau_2) < 0$ , which implies that  $-Z_2(\tau_2) > 0$ . Thus, the sign of  $T'(\tau)$  matches that of  $(c(a^w - K) + c^w)$  [Terman et al. use  $\lambda_1$  to denote  $c$ ]. By showing that this quantity is negative for all relevant  $\tau$  for  $K < a_-$  (Case I in [32]), Terman et al. achieve a sufficient condition for compression in the silent phase.

In general, one can compute the signs of  $a, b, c$  as well as  $a^w, b^w, \dots$  (see e.g. Lemma 1) and then can use (B6), (B8) to derive compression conditions for the silent phase. Simplifications facilitate this process in certain cases even for complex cells. For example,  $\sigma = \sigma' = 0$  during the silent phase for  $E$  cells in a globally inhibitory network as well as for much of the silent phase for mutually coupled cells with fast synaptic decay. In the latter case, however, an adjustment must be made to compensate for the fact that one cell loses inhibition before the other; we omit details and explicit computations here.

## REFERENCES

1. T. Bal and D.A. McCormick, *What stops synchronized thalamocortical oscillations?*, *Neuron* **17** (1996), 297-308.
2. P. Bush and T. Sejnowski, *Inhibition synchronizes sparsely connected cortical neurons within and between columns of realistic network models*, *J. Comp. Neurosci.* **3** (1996), 91-110.
3. C.C. Chow and J. Ritt, *Phaselocking in weakly heterogeneous neuronal networks*, preprint.
4. D. Contreras and M. Steriade, *Spindle oscillation in cats: the role of corticothalamic feedback in a thalamically-generated rhythm*, *J. Physiol.* **490** (1996), 159-179.
5. A. Destexhe, A. Babloyantz, and T.J. Sejnowski, *Ionic mechanisms for intrinsic slow oscillations in thalamic relay and reticularis neurons*, *Biophys. J.* **65** (1993), 1538-1552.
6. A. Destexhe, D.A. McCormick, and T.J. Sejnowski, *A model for 8-10 Hz spindling in interconnected thalamic relay and reticularis neurons*, *Biophys. J.* **65** (1993), 2474-2478.
7. A. Destexhe, T. Bal, D.A. McCormick, and T.J. Sejnowski, *Ionic mechanisms underlying synchronized oscillations and propagating waves in a model of ferret thalamic slices*, *J. Neurophysiol.* **76** (1996), 2049-2070.
8. A. Destexhe and T.J. Sejnowski, *Synchronized oscillations in thalamic networks: insights from modeling studies*, in *Thalamus*; Edited by M. Steriade, E.G. Jones, and D.A. McCormick (1996).
9. U. Ernst, K. Pawelzik, and T. Giesel., *Synchronization induced by temporal delays in pulse-coupled oscillators*, *Phys. Rev. Lett.* **74** (1995), 1570-1573.
10. W. Friesen, *Reciprocal inhibition, a mechanism underlying oscillatory animal movements*, *Neurosci. Behavior* **18** (1994), 547-553.
11. W. Gerstner, J.L. van Hemmen, and J. Cowen, *What matters in neuronal locking?*, *Neural Comp.* **8** (1996), 1653-1676.
12. D. Golomb and J. Rinzel, *Dynamics of globally coupled inhibitory neurons with heterogeneity*, *Phys. Rev. E* **48** (1993), 4810-4814.
13. D. Golomb and J. Rinzel, *Clustering in globally coupled inhibitory neurons*, *Physica D* **72** (1994), 259-282.
14. D. Golomb, X.-J. Wang and J. Rinzel, *Propagation of spindle waves in a thalamic slice model*, *J. Neurophys.* **75** (1996), 750-769.
15. D. Golomb, X.-J. Wang and J. Rinzel, *Synchronization properties of spindle oscillations in a thalamic reticular nucleus model*, *J. Neurophys.* **72** (1994), 1109-1126.
16. N. Hagiwara and H. Irisawa, *Modulation by intracellular  $Ca^{2+}$  of the hyperpolarization-activated inward current in rabbit sino-atrial node cells*, *J. Physiol.* **409** (1989), 121-141.
17. A. L. Hodgkin and A. F. Huxley, *A quantitative description of membrane current and its application to conduction and excitation in nerve*, *J. Physiol. (London)* **117** (1952), 500-544.
18. U. Kim, T. Bal, and D.A. McCormick., *Spindle waves are propagating synchronized oscillations in the ferret LGNd in vitro*, *J. Neurophysiol.* **74** (1995), 1301-1323.
19. N. Kopell and G. LeMasson, *Rhythmogenesis, amplitude modulation and multiplexing in a cortical architecture*, *Proc. Nat. Acad. Sci (USA)* **91** (1994), 10586-10590.
20. T. LoFaro and N. Kopell, *Time regulation in a network reduced from voltage-gated equations to a one-dimensional map*, submitted.

21. D. Perkel and B. Mulloney, *Motor pattern production in reciprocally inhibitory neurons exhibiting postinhibitory rebound*, Science **185** (1974), 181-183.
22. J. Rinzel, *A formal classification of bursting mechanisms in excitable systems*, Proceedings of the International Congress of Mathematics, (A.M. Gleason, ed.) AMS (1987), 1578-1593.
23. J. Rinzel, D. Terman, X.-J. Wang, and B. Ermentrout, *Propagating activity patterns in large-scale inhibitory neuronal networks*, Science **279** (1998), 1351-1355.
24. P. Rowat and A. Selverston, *Oscillatory mechanisms in pairs of neurons connected with fast inhibitory synapses*, J. Computational Neuroscience **4** (1997), 103-127.
25. A. A. Sharp, F. K. Skinner and E. Marder, *Mechanisms of oscillation in dynamic clamp constructed two-cell half-center circuits*, J. Neurophysiol. **76** (1996), 867-883.
26. F. Skinner, N. Kopell and E. Marder, *Mechanisms for oscillation and frequency control in networks of mutually inhibitory relaxation oscillators*, J. Computational Neuroscience **1** (1994), 69-87.
27. D. Somers and N. Kopell, *Rapid synchronization through fast threshold modulation*, Biol. Cyber. **68** (1993), 393-407.
28. M. Steriade, D.A. McCormick and T.J. Sejnowski, *Thalamocortical oscillations in the sleeping and aroused brain*, Science **262** (1993), 679-685.
29. M. Steriade, D. Contreras, F. Amzica, *Synchronized sleep oscillations and their paroxysmal developments*, TINS **17** (1994), 199-208.
30. M. Steriade, E.G. Jones and R.R. Llinás., *Thalamic Oscillations and Signaling*, Wiley, New York; 1990.
31. M. Steriade, R. Curró Dossi, and A. Nunez, *Network modulation of a slow intrinsic oscillation of cat thalamocortical neurons implicated in sleep delta waves: cortically induced synchronization and brainstem cholinergic suppression*, Journal of Neuroscience **11** (1991), 3200-3217.
32. D. Terman, N. Kopell and A. Bose, *Dynamics of two mutually coupled inhibitory neurons*, Physica D **117** (1998), 241-275.
33. D. Terman, N. Kopell and A. Bose, *Functional reorganization in thalamocortical networks: Transition between spindling and delta sleep rhythms*, P.N.A.S. **93** (1996), 15417-15422.
34. D. Terman and E. Lee, *Partial synchronization in a network of neural oscillators*, SIAM J. Appl. Math. **57** (1997), 252-293.
35. D. Terman and D.L. Wang, *Global competition and local cooperation in a network of neural oscillators*, Physica D **81** (1995), 148-176.
36. R.D. Traub and R. Miles, *Neuronal Networks of the Hippocampus*, Cambridge University Press, New York (1991).
37. C. van Vreeswijk, *Partial synchronization in populations of pulse-coupled oscillators*, Phys. Rev. E **54** (1996), 5522-5537.
38. C. van Vreeswijk, L. Abbott and G.B. Ermentrout, *When inhibition, not excitation synchronizes neural firing*, J. Comp. Neuroscience (1994), 313-321.
39. D.L. Wang and D. Terman, *Locally excitatory globally inhibitory oscillator networks*, IIIE Trans. Neural Nets. **6** (1995), 283-286.
40. D.L. Wang and D. Terman, *Image segmentation based on oscillatory correlation*, Proc. of World Congress on Neural Net. (1995), 521-525.
41. X.-J. Wang and J. Rinzel, *Oscillatory and bursting properties of neurons*, in The Handbook of Brain

Theory and Neural Networks; Edited by Michael A. Arbib (1995), 686-691.

42. X.-J. Wang and J. Rinzel, *Alternating and synchronous rhythms in reciprocally inhibitory model neurons*, Neural Comp. **4** (1992), 84-97.
43. X.-J. Wang and J. Rinzel, *Spindle rhythmicity in the reticularis thalamic nucleus: synchronization among mutually inhibitory neurons*, Neuroscience **53** (1993), 899-904.
44. X.-J. Wang, D. Golomb, and J. Rinzel, *Emergent spindle oscillations and intermittent burst firing in a thalamic model: specific neuronal mechanisms*, Proc. Natl. Acad. Sci. (USA) **92** (1995), 5577-5581.
45. M.A. Whittington, R.D. Traub, and J.G.R. Jefferys, *Synchronized oscillations in interneuron networks driven by metabotropic glutamate receptor activation.*, Nature **373** (1995), 612-615.
46. J. White, C.C. Chow, J. Ritt, C. Soto and N. Kopell, *Synchronization and oscillatory dynamics in heterogeneous, mutually inhibited neurons*, J. Computational Neuroscience (to appear).

### Figure Captions

**Figure 1:** Nullclines of simple and complex cells. A) The  $v$ - and  $w$ -nullclines of a simple cell intersect at  $p_0$ , on the middle branch of the  $v$ -nullcline, in the oscillatory case. Bold curve indicates a singular periodic orbit, with double arrows denoting fast pieces and single arrows denoting slow pieces. B) The  $v$ -nullcline and a singular solution of an excitable complex cell with a stable critical point  $p_0$ .

**Figure 2:** Unstable synchronous solutions for mutually coupled simple cells. A) A singular synchronous periodic orbit for coupled excitable simple cells with indirect synapses; dark circles indicate fixed points on  $\mathcal{L}_0, \mathcal{L}_{\sigma_A}$ . B) The dashed line indicates a singular synchronous periodic solution for coupled oscillatory simple cells with direct synapses. This solution is unstable: when one cell jumps up, the other cell jumps to  $\mathcal{L}_{\sigma_A}$ . C) Instability in the singular synchronous periodic solution for coupled oscillatory simple cells with indirect synapses. Cell 1 follows the  $-\cdot-\cdot-$  path while cell 2 follows the  $-\cdot-\cdot-\cdot-$  path. Cell 1 jumps up first; subsequently, cell 2 becomes inhibited first and thus falls farther behind cell 1.

**Figure 3:** Singular solutions for complex cells. A) The slow phase space of an uncoupled complex cell, bounded by the jump-up curve  $J_L$  and the jump-down curve  $J_R$  of the slow manifold  $\mathcal{C}_s$ . The solid (dashed) curves represent evolution in the silent (active) phase.  $P_0$  is a stable fixed point. B) Numerically generated synchronous solution for mutually coupled complex cells that are separately excitable, in  $(y, w)$ -space. These curves, as well as those in other figures, were generated using the program XPPAUT, developed by G. B. Ermentrout, with parameter values given in Appendix A. The solid curve is the solution, the dashed curves are the jump-up (labeled) and jump-down (approximately horizontal, unlabeled) curves for  $s = 0.2$ , and the dash-dotted curves are those for  $s = \sigma_A = 0.8$ . Note that the curves for  $s = 0.8$  lie at larger  $w$ -values than those for  $s = 0.2$ . Since  $\epsilon \neq 0$ , the synchronous solution does not jump up [ $y' = 0$ , near  $(y, w) = (0.08, 0.07)$ ] immediately upon reaching the jump-up curve.

**Figure 4:** Compression mechanisms for mutually coupled complex cells. A) Compression in the time-metric  $\rho_w$  can occur between mutually coupled complex cells in the jump up. Note that  $w_1(0) < w_2(T_0)$  and  $y_1(T_0) > y_2(0)$ . The Euclidean distances  $d_w(0), d_w(T_0)$  are used to compute the time metrics  $\rho_w(0), \rho_w(T_0)$ , respectively. B) A reversal of orientation in the active phase (solid lines) can lead to compression in the jump down; dashed line indicates evolution of cell 1 in the silent phase. C) Numerically computed trajectories of a pair of mutually coupled complex cells undergoing order reversal. Cells 1,2 correspond to  $c_1, c_2$  respectively in B). Parameter values are given in Appendix A.

**Figure 5:** Nullclines for A)  $E$ -cells and B)  $J$ -cells in a globally inhibitory network with simple cells. The heavy lines and points  $P_i, Q_i$  correspond to the singular synchronous solution discussed in the text. Note that  $s_J$  decays on the slow time scale.

**Figure 6:** The slow phase plane for an  $E$ -cell. The curve  $w_L(s_J)$  is the jump-up curve, which trajectories reach if  $K_J$  is large enough ( $-\cdot-\cdot-$  path; cell jumps up from the point marked as ‘\*’). The dotted curve  $W_F(s_J)$  consists of zeros of  $G_L(w, s_J)$  in system (5B.1); trajectories tend to the stable critical point  $W_F(0)$  as  $s_J \rightarrow 0$  for small  $K_J$  ( $-\cdot-\cdot-\cdot-$

path). Note that  $w' < 0$  for  $w > W_F$ .

**Figure 7:** Three-dimensional slow phase space for a singular synchronous periodic orbit of the globally inhibitory network. Double (single) arrows denote evolution on the fast (slow) time scale, solid (dashed) lines indicate the silent (active) phase, and points  $P_i$  are as discussed in the text. The shaded region represents the jump-up surface  $w = w_L(y, s_J)$ .

**Figure 8:** Numerical solution, with two TC clusters, of the thalamic network [parameter values given in Appendix A]. Voltages are in  $mV$  and time is in  $msec$ . A) RE cell (the time course of which matches that of the RE population of 3 cells). B) TC population of 6 cells, forming two clusters of three cells each. C) Inhibitory synaptic variables  $s_A$  (dashed) and  $s_b$  (solid); note that  $s_b \equiv 0$ , since the RE cell bursts are not powerful enough to activate slow inhibition in this case.

**Figure 9:** Numerical synchronous solution of the thalamic network [parameter values given in Appendix A]. Voltages are in  $mV$  and time is in  $msec$ . A) RE cell (the time course of which matches that of the RE population of 3 cells). B) TC population of 6 cells (synchronized). C) Inhibitory synaptic variables  $s_A$  (dashed) and  $s_b$  (solid); note that  $s_A$  turns on and off faster than  $s_b$ , which in turn stays on longer.

**Figure 10:** Numerical trajectory of a TC cell, together with jump-up surface of knees (shaded), in the  $(h, r, s_b)$  slow phase space. The TC cell shown belongs to the synchronized population of 6 TC cells shown in Figure 9. Note that  $s_b$  does not immediately increase when the cell jumps up, since we have taken slow inhibitory synapses to be indirect.

**Figure 11:** Numerical trajectory of a TC cell, together with jump-up surface of knees (shaded), in the  $(h, r, s_A)$  phase space. The TC cell shown belongs to one of the clusters of the solution shown in Figure 8. We use  $s_A$  rather than  $s_b$  since slow inhibition is not activated in this solution. The trajectory shown jumps up to the active phase only once, after passing a bit through the jump-up surface (since  $\epsilon \neq 0$ ). When it comes close to the jump-up surface a second time, it is inhibited by the jumping of the other cluster (not shown); hence,  $s_A \rightarrow 1$  but  $h, r$  continue to increase.

**Figure 12:** The set-up for analysis of compression in the silent phase in two dimensions (i.e., assuming  $s$  is fixed); the picture generalizes naturally to 3-d when  $s$  is included as another slowly evolving variable. Cell 1 jumps up first, with  $\tau = T_1$ , at  $(y_1^*, w_1^*)$ . The larger dotted square shows a blow-up of the smaller dotted square, in which the vectors  $V$  and  $(\eta, \rho)$  are defined.

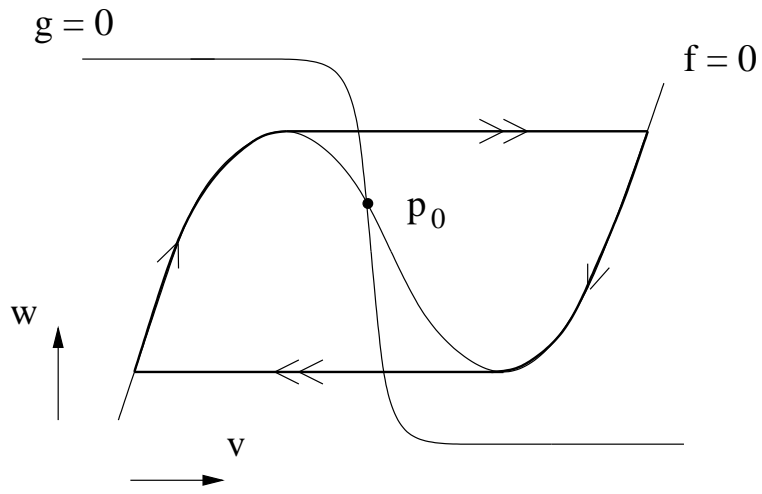


FIGURE 1A

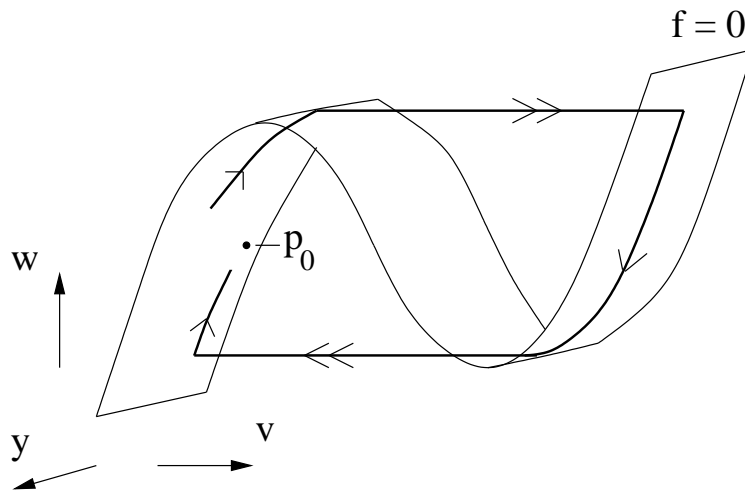


FIGURE 1B

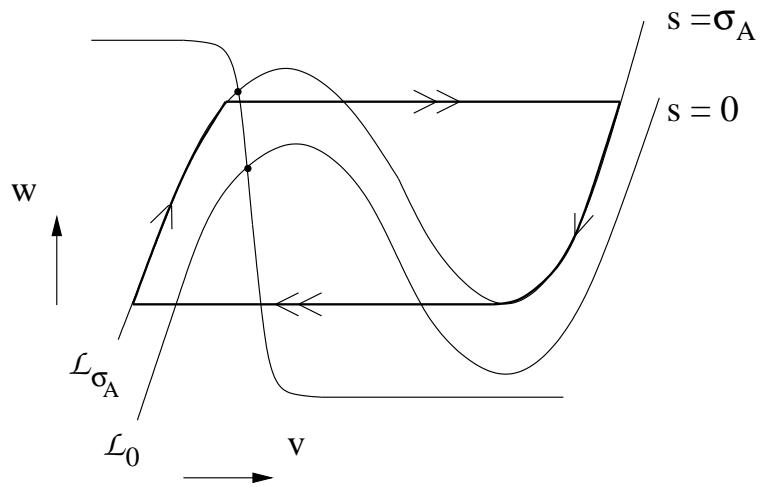


FIGURE 2A

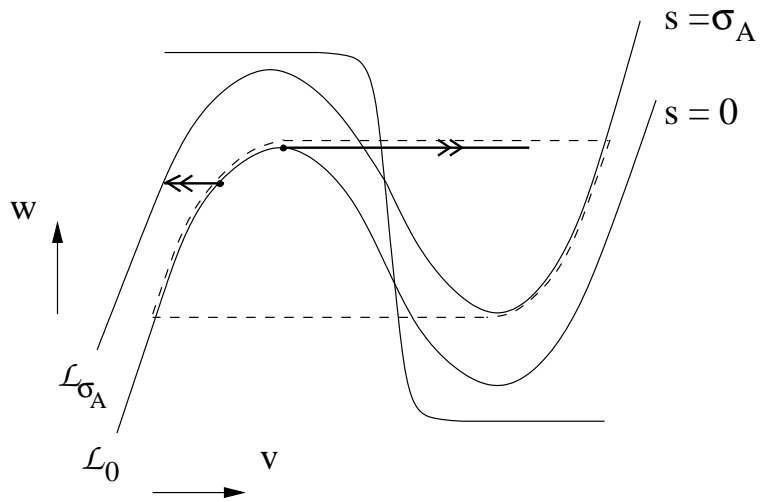


FIGURE 2B

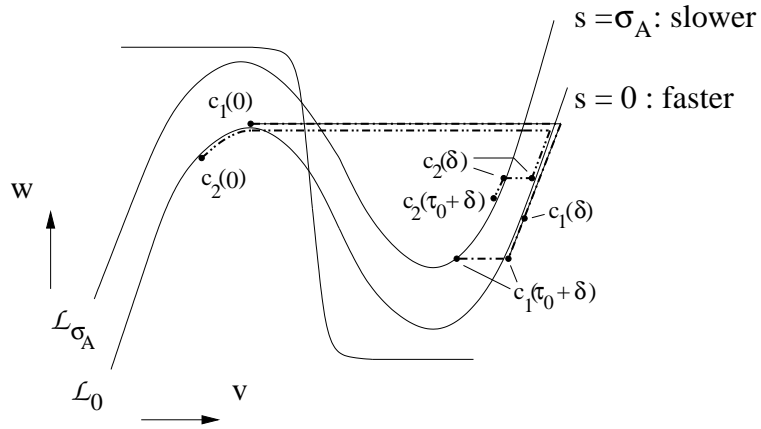


FIGURE 2C

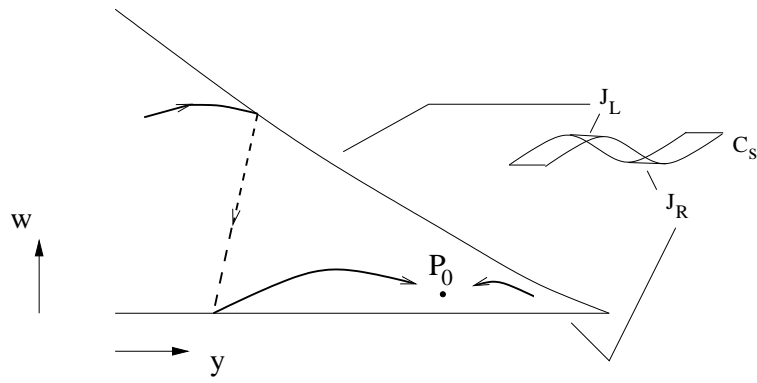


FIGURE 3A

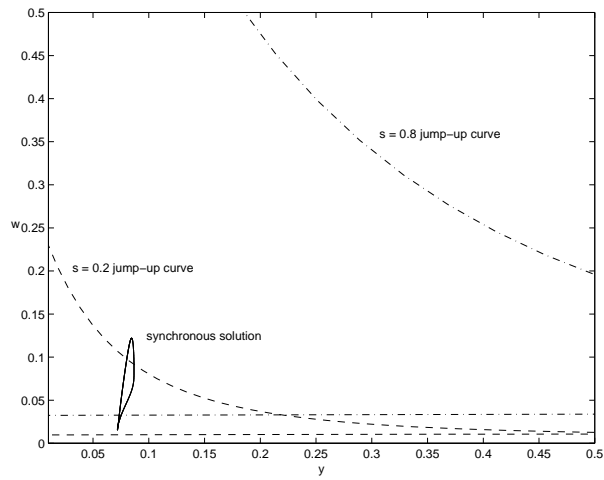


Figure 3B

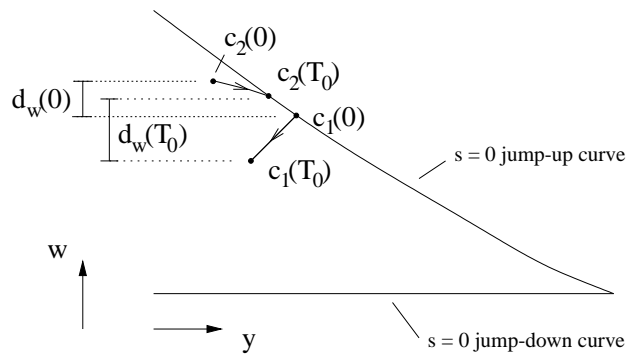


FIGURE 4A

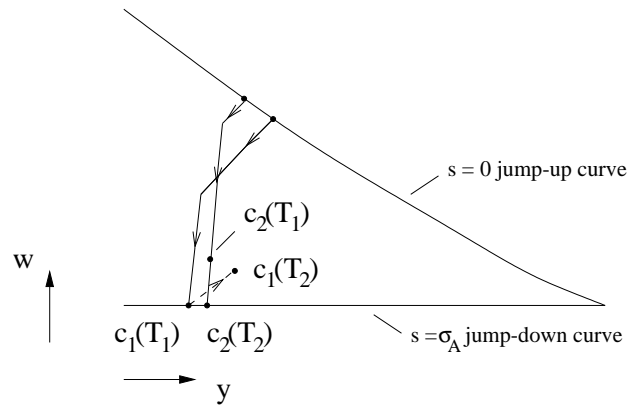


FIGURE 4B

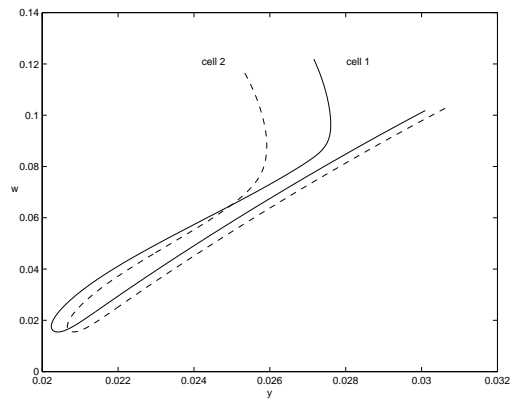


Figure 4C

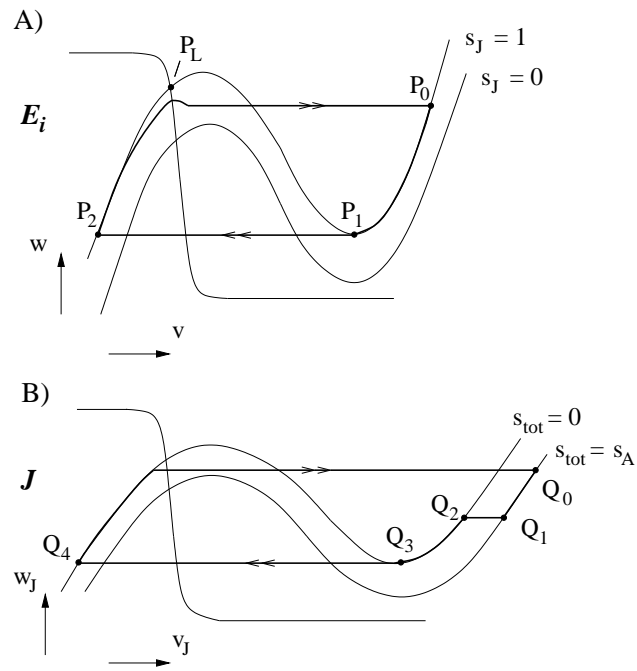


FIGURE 5

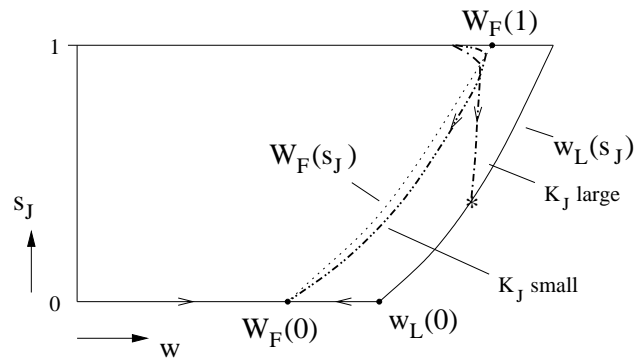


FIGURE 6

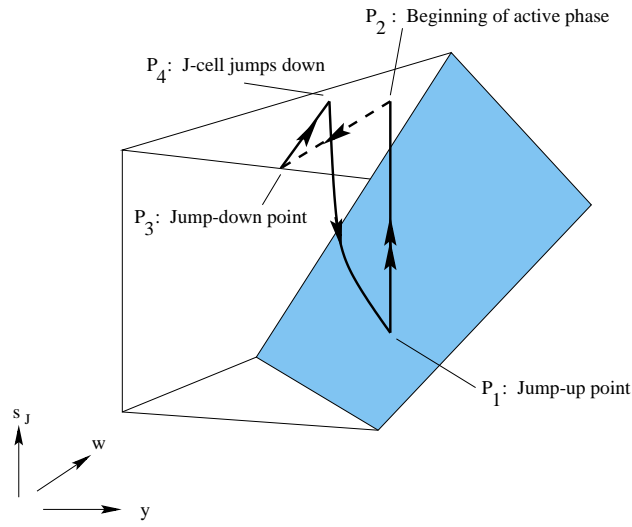
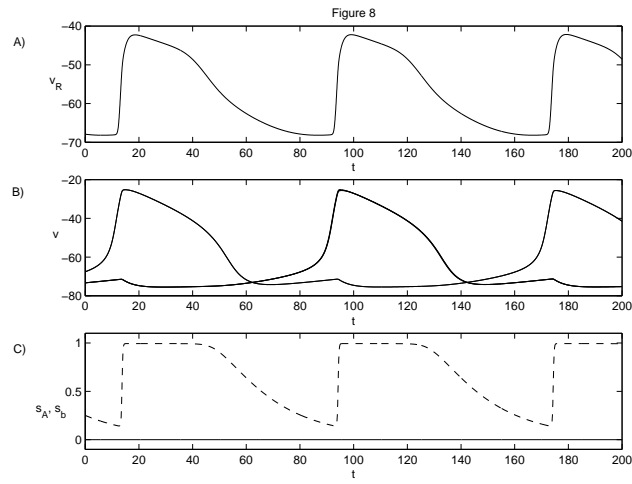
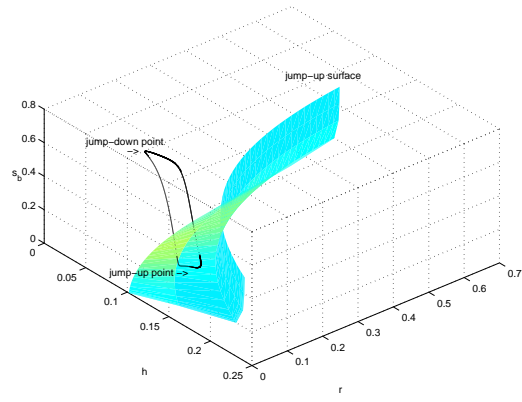
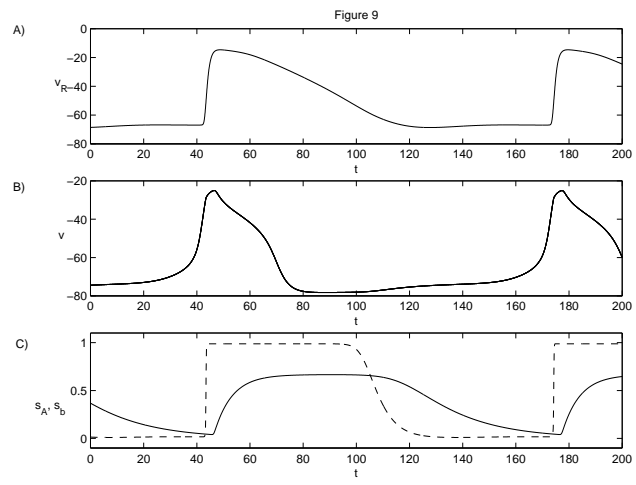


FIGURE 7





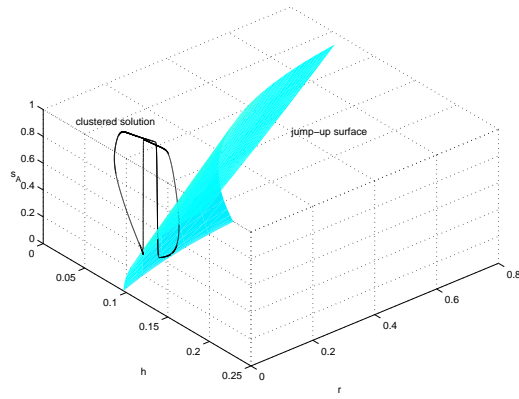


Figure 11

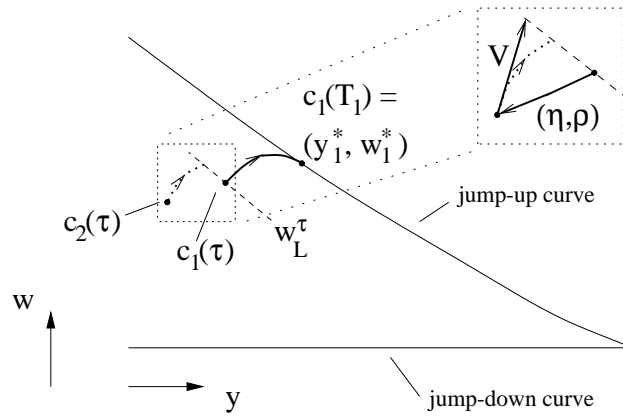


FIGURE 12